Physics – Uspekhi **67** (8) 779 – 802 (2024)

REVIEWS OF TOPICAL PROBLEMS

PACS numbers: 29.40.Gx, **61.85.+p**, 95.55.Vj

ON THE 90TH ANNIVERSARY OF THE P.N. LEBEDEV PHYSICAL INSTITUTE (LPI)

Track technique in present-day physics of atomic nuclei and elementary particles, astrophysics, and nanotechnology

S A Gorbunov, A E Volkov, K I Zhukov, N S Konovalova, N G Polukhina, N I Starkov, T V Shchedrina

DOI: https://doi.org/10.3367/UFNe.2023.10.039585

Contents

Abstract. Track detectors, contributing to the understanding of the structure and properties of matter, are widely used in fundamental and applied research using modern accelerators, in studying the nature of particles of cosmic origin, and for muography. The advantage of the technique is the visibility of the results and the possibility of reconstructing trajectories, interaction vertices, and particle decay points with an accuracy of several microns. Specific features of various experiments, requiring original solutions in their design, data processing, and interpretation, have brought about the multidisciplinary development of the subject. In addition to the tasks of experimental physics, the evolution of the track technique is determined by the problems of innovative technologies and the creation of new materials. These trends can be traced in the work of the Laboratory of Elementary Particles of the Lebedev Physical Institute, which has been using track detectors of various types in its experiments for many decades. The review presents the ideas and results of world-class experimental and modeling studies conducted previously and currently being conducted with the participation of laboratory researchers, as well as those planned for the near future.

Keywords: experiments based on track technique, modeling of track formation processes, methods for processing and analyzing track detector data

S A Gorbunov [a], **A E Volkov** [b], **K I Zhukov** [c], **N S Konovalova** [d], **N G Polukhina** [e], **N I Starkov** [f], **T V Shchedrina** [g]
Lebedev Physical Institute, Russian Academy of Sciences, Leninskii prosp. 53, 119991 Moscow, Russian Federation
E-mail: [a] s.a.gorbunov@mail.ru, [b] a.e.volkov@list.ru, [c] Konstantin.Zhukov@cern.ch, [d] ninakonovalova@yandex.ru, [e] polukhinang@lebedev.ru, [f] starkovni@lebedev.ru, [g] tvshchedrina@gmail.com

Received 30 September 2023, revised 27 October 2023
Uspekhi Fizicheskikh Nauk **194** (8) 826 – 852 (2024)
Translated by V L Derbov

1. Introduction

The Laboratory of Elementary Particles (LEP) of the Lebedev Physical Institute (LPI), Russian Academy of Sciences, was created by A I Alikhanyan in 1943 for studying high-energy particles of cosmic radiation and their interactions [1]. From the moment of its creation to the present day, the work of the laboratory team has been aimed at studying the most urgent problems of modern physics, combining scientific and educational activities, and training new personnel from among graduates of the best physics universities in Russia. Close cooperation is maintained between the experimenters and theoreticians at the laboratory, initiated by A I Alikhanyan, whose friendship with such outstanding theoreticians as L D Landau and I Ya Pomeranchuk resulted in fruitful scientific cooperation [2]. The result of this collaboration was, in particular, the distribution function constructed by L D Landau for fast particles that have passed through a layer of matter of a given thickness and lost energy as a result of ionization collisions [3].

The research activities of LEP are largely based on the tracking technique, which reconstructs particle tracks and their interaction vertices in the detector volume. In the laboratory, the first large Wilson chambers with a volume of up to 40 liters were created, as was the first domestic propane bubble chamber with a volume of 0.75 liters. Under Alikhanyan's leadership, a new type of spark chamber (track spark chamber) was created, which allowed determining the momentum of charged particles in a magnetic field; this work was awarded the Lenin Prize in 1970. Alikhanyan's team members also developed a method of detecting superhigh-energy particles based on transient radiation in the X-ray and optical frequency ranges [4].

The invention of modern accelerators opened up a new stage in the study of elementary particles using track detectors. LEP experimenters traditionally collaborate with the largest international research centers, such as the

European Center for Nuclear Research (CERN), the German Electron Synchrotron DESI (Germany), the Enrico Fermi National Accelerator Laboratory (USA), and the National Gran Sacco Laboratory (Italy), assimilating and creating high-tech detection and measurement instrumentation. This work, experience, and knowledge have enabled LEP researchers, inter alia, to become key performers of the ATLAS experiment, one of the four main experiments at the Large Hadron Collider.

The track technique finds application in a wide range of research, from detecting elementary particles to studying superheavy nuclei, which implies an individual approach to designing experiments, data processing, and analysis. One of the main advantages of the track technique is a high spatial resolution and, as a consequence, the possibility of extracting and identifying the tracks, outgoing from different vertices. Track and vertex reconstruction is a critical component of data analysis in accelerator experiments, including fixed-target experiments, lepton and hadron collider experiments, and neutrino experiments in which the detector is also the target. Integrated track detectors (nuclear emulsion, glasses, micas, plastics, olivines from meteorites, etc.) accumulate the information on particle tracks during the entire exposure time. This feature is a substantial advantage at small fluxes of detected particles; however, it leads to significant difficulties in the processing and analysis of experiments with high particle density, e.g., at colliders.

Among all track detectors used in particle physics, nuclear emulsion detectors possess the highest spatial resolution [5]. After a long pause, interest in nuclear emulsions revived in the 1990s due to achievements in the field of digital data processing with high-speed scanning equipment and progress in the production of new types of emulsions with various grain sizes. The variety of sizes and configurations of emulsion detectors is complemented by the possibility of creating hybrid systems based on them in combination with electronic detectors for time synchronization and/or muon identification [6–8].

The creation of the so-called emulsion cloud chamber (ECC) was a breakthrough in the emulsion technique. This design, which is a multilayer composite of emulsion films with layers of passive material (usually plastic or metal) and positioned perpendicular to the incident particles, is a high-resolution (up to 1 μm) track detector with the ability to reconstruct events in three dimensions. This type of detector was developed in the 1950s to study cosmic rays [9]. In particular, it was used to observe for the first time the decay of charmed particles in a cosmic ray experiment [10], and the DONuT experiment was the first to detect the tau neutrino ν_τ [11]. The ECC principle involves two key parameters necessary to detect particles with an extremely small interaction cross section, namely, a large mass and very high spatial resolution [12]. Based on the ECC technique, hybrid experiments at colliders were developed, combining emulsion and electronic detectors, the latter being used for two purposes: as a trigger signal from an event occurring in the target and for preliminary determination of the region of the possible event in the ECC (see Sections 2.1.3 and 2.1.4).

Processing the data of integrated track detectors is based on analyses of the images obtained by means of automated optical microscopes, whose software can be adapted for operation with all known integrated-type detectors. The first automated scanning microscope in Russia was the PAVICOM (the Russian acronym for Completely Automated Measuring Complex) measurement facility (Section 4), created at LEP, which from the moment of its creation in the late 1990s has been successfully used to process experimental material from large international and Russian projects.

This review is devoted to describing the most important experimental and modeling studies conducted with the participation of LEP researchers.

Section 2 briefly describes the most significant international and domestic experiments with the participation of LEP researchers, based on the track technique. Section 3 is devoted to models of forming etched tracks of fast heavy ions in solid-state track detectors. Section 4 describes the PAVICOM automated scanning facility, at which the data from LEP experiments using track detectors are processed based on modern technologies.

2. Experiments based on track technique at Laboratory of Elementary Particles

2.1 Accelerator experiments

2.1.1 Detector of transient radiation for ATLAS experiment at Large Hadron Collider at CERN. On June 5, 2022, the Large Hadron Collider (LHC) restarted after a break of more than three years for maintenance and upgrade work. The protons circulated in opposite directions collide at an energy of 13.6 TeV in the center-of-mass reference frame with a frequency of 40 MHz. This run, the so-called RUN3, started the process of collecting experimental data for the New Physics.

The ATLAS (A Toroidal LHC ApparatuS) experiment [13] is one of the four basic experiments at LHC. It is aimed at the search for superheavy elementary particles, including those beyond the framework of the Standard Model (SM). The detector, having the same name, is 2×40 m in size and located underground at a depth of about 100 m and is a cylindric construction formed by various detecting subsystems, the inner radius of which is a few centimeters from the point of interaction of colliding protons. An exterior view of the ATLAS facility is shown in Fig. 1.

In the center of the facility, there is an inner detector 2.1 m in diameter and more than 6 m long in a magnetic field of 2 T. The detector consists of three sensor systems (Fig. 2): a pixel detector, a microstrip semiconductor tracker (SCT), and a transition radiation tracker (TRT). It is intended for identifying charged particles and reconstructing their trajectories from the interaction vertex to the calorimeter. Due to the magnetic field, the trajectories of charged particles curve, which allows determining their charge and momentum with high accuracy.

The constitutive systems include two types of detectors: silicon, based on silicon chips (pixel and strip detectors), and gas, based on drift tubes (transient radiation detector). The detectors are arranged so that the particles intersect them predominantly perpendicular to the plane of the chip or the axis of the tube. To reduce the intrinsic noise, the silicon part of the detector is placed in a cryostat, which is separated from the TRT detector of transient radiation, operating at a normal temperature. The system of SCT silicon detectors allows obtaining six track coordinates; 30 more coordinates are determined by means of the system of TRT detectors of transient radiation. The accuracy of track reconstruction in the inner detector amounts to 150 microns.

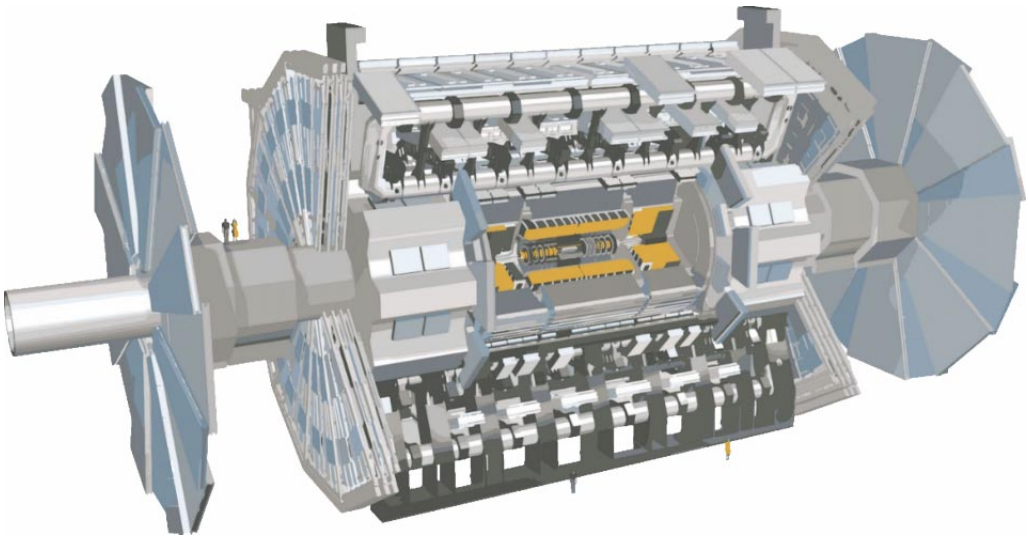

Figure 1. 3D model of ATLAS setup at the Large Hadron Collider.

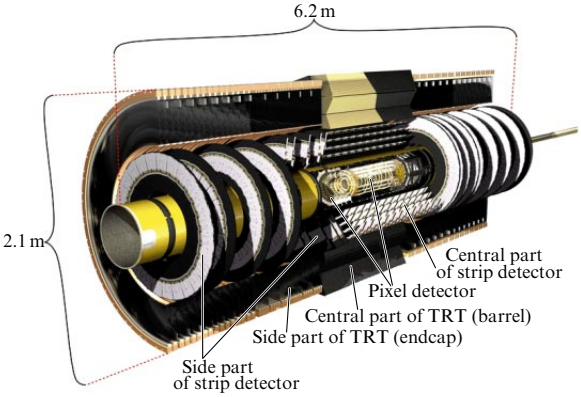

Figure 2. Schematic diagram of inner detector of ATLAS experiment.

The TRT is the inner detector component most remote from the beam axis. It is a combination of a track detector and a detector of transient radiation, capable of both track reconstruction and identification of electrons in the flow of produced particles [14]. The TRT detector consists of three parts: the central barrel and two end cups. In the central part, there are gas-filled drift tubes (straws) 4 mm in diameter and 144 cm long, directed along the beam axis. The anode filament of each straw is divided in the middle by a glass isolator, which allows taking a signal from each half of the straw independently, thus doubling the number of information channels. As a result, the barrel part incorporates 105,088 information channels. The voltage is applied to the cathode (tube), which reduces twice the number of high voltage supply channels, as well as simplifies the supply electric circuit when taking information from the anode. The end parts of the detector are wheel-shaped with radially directed tubes 37 cm long. Under the action of a particle passing through, the gas in a straw is ionized, forming an electric pulse. This makes it possible to know the straws through which the particle trajectory has passed.

In addition to reconstructing the charged particle tracks, the TRT detector can identify electrons against the hadron background due to the transient radiation effect. For this purpose, a radiator is installed in the TRT, which is a stack of polypropylene films (in the end part of the detector) or fibers (in its central part) with a different permittivity from that of the medium, filling the space between the tubes. Due to such radiator construction, the particle multiply crosses interfaces separating media with different permittivity values. When a charged particle passes, transient radiation arises at the interface between materials, giving rise to additional energy release, which for electrons form signals of higher amplitude, allowing their identification. Thus, the reading electronics have two trigger thresholds: a low one for detecting the coordinates of a particle and a high one for its identification. The signal in a straw from a quantum of transient radiation created when an electron passes through the radiator exceeds the upper discrimination threshold.

Transient radiation was predicted by LPI scientists, academicians V L Ginzburg and I M Frank [15], and experimentally discovered by A I Alikhanyan [4]. From the late 1970s, the LEP team (led by A P Shmelev) together with colleagues from MEPhI (led by B A Dolgoshein) started to work with detectors of transient radiation. The team worked with detector prototypes on test beams and took part in the NA34 Helios international experiment (CERN, 1984–1989) with a detector of transient radiation for identification of electrons at the fast trigger lever [16]. The team's experience allowed them to join the development of detectors of the new generation at the Large Hadron Collider, where it was proposed to use a part of the tracker for identification of electrons. As a result, LEP researchers began the work on creating and maintaining the TRT in the ATLAS collaboration, participating in the assemblage of the tracker prototypes and work during sessions on test beams of the Super Proton Synchrotron (SPS) accelerator. Notably, in the course of assembling the end wheels of the TRT detector, the anode filaments were installed in all 150 thousand straws. Before assembling the detector, each of the 28 wheels underwent a testing procedure that included electrical testing (detecting leaks and high voltage breakdowns), electronics testing, and gas testing (searching for possible leaks and blowing). After validation, the detector wheels were gathered in stacks by 14 pieces, forming the so-called endcups A and C (in correspondence with the names of the sides of the ATLAS experiment shaft) placed at the ends of the central part of the detector.

When constructing the detector, extremely complex devices were developed to ensure its operability, particularly many drift tubes, the creation of which required developing a unique system of high-voltage supply. While testing the detector prototypes, technical requirements regarding high-voltage supply sources were formulated. Since it was impossible to find a suitable serial industrial product, the necessary system was created at the Joint Institute for Nuclear Research (JINR) under the supervision and with the participation of LEP staff members [17]. The system consists of 2000 channels, each providing a supply of 192 straws (a voltage of 1.5 kV with an accuracy of 0.1%) and is protected against breakdowns. Upon an electric breakdown inside a straw, the tube surface may be damaged, due to which a threat of leakage of the filling gas through the formed hole arises. In this case, it is necessary to promptly switch off the power supply. The system of protection against breakdowns evaluates the integral breakdown current in 40 ms and, if the breakdowns do not stop, the high-voltage supply is switched off. During 10 years of operation, the system of protection against breakdowns demonstrated its high reliability, requiring no serious intervention except minor repairs of individual channels.

The TRT detector working gas is an $Xe + CO_2 + O_2$ mixture in the proportion of 70%–27%–3%. The main component, Xe, ensures efficient absorption of gamma quanta of the transient radiation. Initially, tetrafluoromethane CF_4 gas was used as a stabilizing addition instead of oxygen, but it was revealed that it damages glass isolators of the filaments of the barrel part, due to which it had to be abandoned. Since the signal shape, drift rate, and gas amplification directly depend on the purity of the gas mixture, the TRT gas system includes active control of the gas composition, ensuring the stability of detector operation. Due to the high cost of Xe, the system operates in the circulation mode. Extensive experience working with gas mixtures allowed the LEP researchers to contribute substantially to the system development, tuning, and further maintenance.

In addition to reliable equipment, efficient software capable of fast upgrade by the developers, if necessary (e.g., when the parameters of the detecting equipment change), is a key element of any working experiment. The major goal for the inner detector software is to reconstruct the tracks of charged particles, which produce signals in the main constituent components, pixel and strip silicon counters, and the detector of transient radiation.

LEP specialists made a key contribution to the development and support of the track reconstruction program, which has been used already for almost 10 years and provides stable, high quality, and fast reconstruction of events. Currently, the work on optimization of the track reconstruction program is in progress for the new version of the inner detector geometry, which is planned for use in the next phase of LHC work to begin in 2026. At this stage of LHC operation, it is planned to increase the luminosity to 7.5×10^{34} cm^{-2} s^{-1}, which nearly corresponds to 200 proton-proton collisions in each interaction of colliding beams. In addition, the region of rapidity of the particles under study will increase from 2.6 to 4. In this modification of the experiment, the multiplicity of the created particles will exceed that observed in RUN3 by approximately six times. The high-efficiency operation under new conditions will require developing upgraded inner detector and the appropriate software. A new version of the program

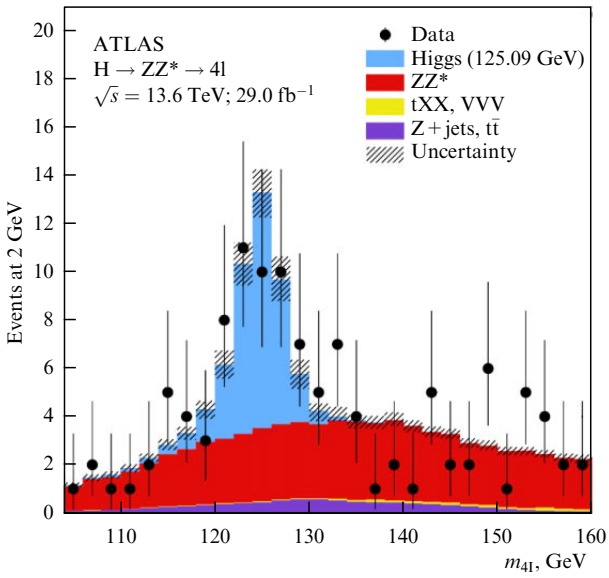

Figure 3. Mass peak of Higgs boson from decay into four leptons (blue) against a background of other suppressed events [19].

for track search and reconstruction has been already approved in the course of optimizing new silicon strip and pixel detectors (the ATLAS ITk project [18]), which will replace those operating within ATLAS now.

One of the priority tasks of the Large Hadron Collider physical program is searching for and studying the Higgs boson, the chronologically last particle of the SM. In the process of the search, the following probable channels of Higgs boson decay were considered:

- $pp \to H \to \gamma\gamma$,
- $pp \to H \to ZZ^* \to 4l\,(l = e, \mu)$,
- $pp \to qqH \to qq\tau^+\tau^-$,
- $pp \to H \to W^+W^- \to l\nu l\nu, l\nu qq$
- $pp \to t\bar{t}H \to t\bar{t}b\bar{b}$,
- $pp \to t\bar{t}H \to t\bar{t}W^+W^-$,
- $pp \to ZH \to l + l - W^+W^-$.

In each of these channels, information about the tracks of charged particles from the inner detector data was analyzed. In the decay channel with the creation of four leptons, the results of identification of electrons in the TRT detector were used. This decay channel was used in ATLAS to determine the mass of the Higgs boson in 2012 [19]. Figure 3 shows the histogram with the mass peak from the Higgs boson in the region of 125.09 GeV.

LEP researchers take part in the analysis of the experimental data obtained at the ATLAS facility. In particular, the study of $W \to J/\psi + D_s$ decay is being carried out, which will allow specifying the W boson mass or getting a new limitation on its mass. Urgent problems of searching for the New Physics beyond the SM are being solved. It is known that in the SM the so-called lepton universality is considered, when the interaction of leptons via gauge bosons is invariant with respect to the flavor of the former. The flavor-changing neutral current (FCNC) processes provide ideal conditions for checking lepton universality. The SM forbids FCNC at the level of tree Feynman diagrams and allows only amplitudes including electroweak loop (penguin and box) Feynman diagrams. Such transitions are rare and sensitive to new particles. The presence of such particles can lead to a significant discrepancy between the rates of individual decays

and the SM predictions or to a change in the angular distribution of the decay particles in the final state. Thus, the detection of this kind of effect can be indirect proof of the presence of new particles when the masses of the new particles are inaccessible for the LHC.

A group of LEP researchers continues to actively participate in the ATLAS experiment, ensuring the stable operation of the TRT detector. After the end of the RUN3 session of the Large Hadron Collider in 2026, the disassembly of the existing inner detector will begin, instead of which a new tracker will be installed, completely based on silicon detectors capable of operating under the high-load conditions. This stage of the collider operation will be called High-Lumi. LPI plans to take part in this new phase of the experiment, based on the accumulated experience in the field of creating detectors of charged particles and processing the obtained data.

2.1.2 EMU-15 experiment. Experiments on the physics of elementary particles occupy a significant place in LEP research. One such experiment, EMU-15, was carried out at CERN in 1996 on a beam of Pb ions with an energy of 32 TeV per nucleus (158 GeV/nucleon), obtained at the SPS accelerator [20, 21]. The EMU-15 collaboration consisted of Russian participants only and in this aspect was unique for CERN. The aim of the work was to study collective effects and features of projection of secondary particles in central collisions of accelerated Pb nuclei with the nuclei of a Pb target. The criterion for selecting central events was the large multiplicity of the secondary charged particles and the absence of fragments with $Z \geqslant 2$. Based on the obtained data, studies of nuclear matter properties were carried out at superhigh densities and temperatures, in particular, the analysis of possible manifestations of such states of matter as quark-gluon plasma [22].

During the experiment, 16 emulsion chambers were sequentially irradiated. Each chamber was a cylinder 26 mm long and 95 mm in diameter and contained a thin (400 μm) Pb target and 38 layers of double-sided nuclear emulsion, the first of which was located directly in front of the target and the rest behind it (Fig. 4).

The axis of the cylindrical chamber was directed along the beam; during the irradiation, the chamber was placed in a transverse magnetic field of 2 T. Such a design of the experiment allowed determining three components of momenta and the charge signs of the secondary particles.

The total number of ions passed through the chamber during one exposure was $\sim 10^4$ particles. In each chamber, about 10 central Pb–Pb interactions were found with a multiplicity of more than 10^3 secondary charged particles. Processing events with so high a multiplicity, implying the execution of millions of coordinate measurements of tracks in the nuclear emulsion, required creating automated instrumentation to accelerate the processing a great deal. Especially for processing the data of the EMU-15 experiment, a completely automated measuring system, PAVICOM (Section 4), was developed at LEP, which combined the optical facility based on the MPE-11 microscope (LOMO) with the fast CMOS camera and automated the scanning table, computer-driven via a controller [23]. The work with PAVICOM required developing software to control the movement of the microscope table, acquiring and analyzing images, and reconstructing the geometric pattern of the secondary charged particle projection.

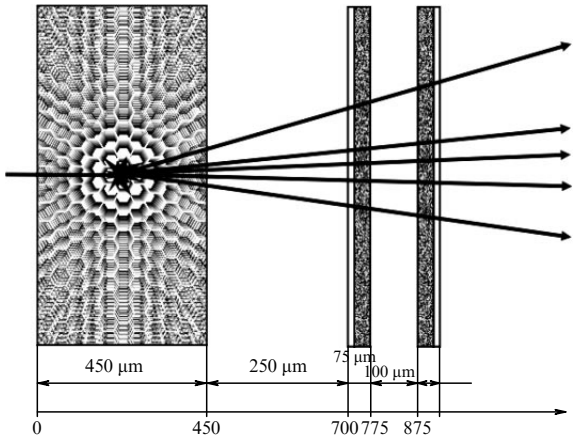

Figure 4. Schematic diagram of recording interaction products in emulsion chamber. Diagram shows a lead target and two of the 37 emulsion layers located behind it.

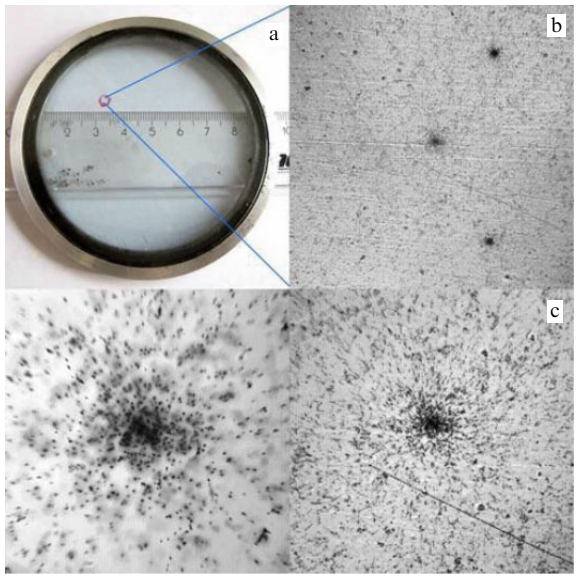

Figure 5. (a) Emulsion plate of EMU-15 experiment. (b) Central field of view at 8× objective magnification (field of view of 820 × 820 μm). In the center, traces of Pb nuclei have not yet dispersed and are concentrated very densely, which makes central region the darkest. Traces of noninteracted Pb nuclei are visible in image. (c) Same field of view at magnification 20× (right, field of view of 330 × 330 μm) and 60× (left, field of view of 115 × 115 μm).

Images of particle traces at the output of the video camera are formed by groups of pixel clusters of different degrees of darkness and look like aggregates of grains against a grey background (Fig. 5). The task of track reconstruction from a given set of clusters was solved using the least squares method.

To construct the pseudorapidity distribution of secondary charged particles, the tracks in the adjacent emulsion layers were 'sewed' and the trajectory of each particle was reconstructed passing through the layers of the nuclear emulsion after the interaction. To determine the pseudorapidity of the formed particles, an iteration procedure for determining the event axis was executed; the reconstructed event axis was accepted as the direction of motion of the Pb nucleus that caused the interaction.

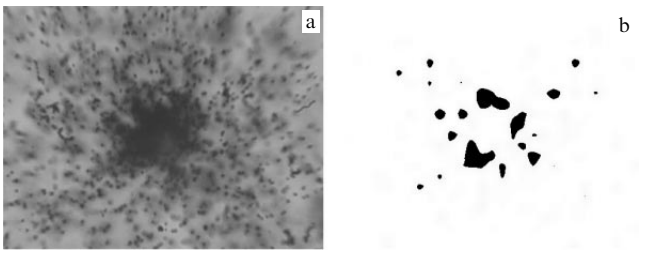

Figure 6. (a) Event 5c15e generated by central Pb–Pb interaction in a nuclear emulsion, magnification 90×; (b) target diagram of event 5c15e after four iterations of wavelet transform [26]. Central part of interaction was excluded from analysis due to indistinguishability of particles.

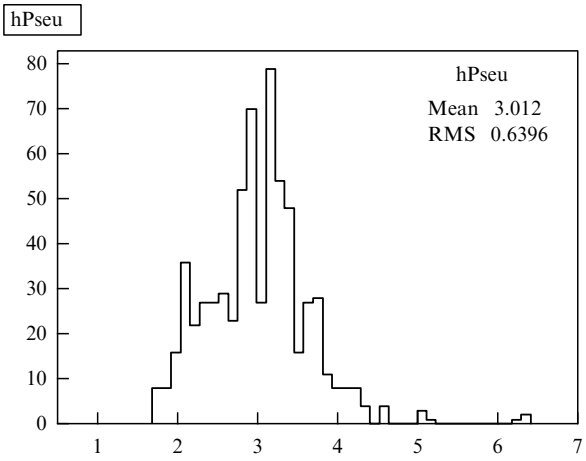

Figure 7. Pseudorapidity distribution of secondary charged particles from 5c15e event [26].

The analysis of characteristics of the produced particles in the phase space, making it possible to reach a conclusion about the process dynamics, included the construction of pseudorapidity distribution of secondary particles and a subsequent wavelet analysis of the distribution [24]. The wavelet analysis allows revealing the clustering phenomena in the processes of multiple creation, selecting the most significant fluctuations that exceed the statistical component [25]. To analyze the characteristics of the relativistic nuclei interaction in the EMU-15 experiment, the wavelet analysis was applied for the first time in the physics of elementary particles and high energy physics.

Figure 6a shows the central part of the 5c15e event in the nuclear emulsion (the multiplicity of charged particles is about 1500 particles) and its target diagram after four wavelet transform iterations (Fig. 6b), in which the correlation anisotropy in the azimuthal angle is clearly seen in the form of a characteristic ring arrangement of a certain subsystem of particles in the target plane. The origin mechanism of the observed ring structures can be explained by an analog of Cherenkov radiation that occurs when an object moves in a medium with a velocity exceeding the phase velocity of perturbation propagation in this medium (with gluons as an analog of photons).

The most significant feature of the ring structure existence is the presence of two peaks in the pseudorapidity distribution of the secondary particles. The pseudorapidity distribution of particles in the 5cl5e event has two peaks (Fig. 7), which correspond to two cones of particle projection (forward and backward in the center-of-mass frame). The detection of such structures is of great interest, since they can evidence in favor of the manifestation in strong interactions of a mechanism related to the gluon analog of Cherenkov photon radiation [27].

2.1.3 OPERA experiment. The accelerator experiment using the largest amount of nuclear emulsion, in which LEP staff members were active and competent participants, was the OPERA (Oscillation Project with Emulsion tRacking Apparatus) experiment aimed at searching for neutrino oscillations, which was carried out from 2008 to 2012 [12]. OPERA was the first experiment on direct registration of the tau neutrino ν_τ appearance in a beam of muon neutrinos ν_μ (the first 'on the appearance' experiment).

The detector of the OPERA experiment was located in the underground laboratory LNGS (Laboratori Nazionali del Gran Sasso, Italy) at a depth of about 1400 m at a distance of 730 km from the source of a beam of muon neutrinos with the mean energy of 17 GeV at CERN (Fig. 8).

Tau neutrinos were recorded by detecting a τ lepton created in the interaction of ν_τ in the OPERA detector. The criterion for event selection was the absence of a muon in the final state. The experiment was carried out under conditions of a low background with a signal-to-noise ratio of the order of 10.

In the OPERA experiment, the neutrinos interacted in a massive target made of lead plates, sandwiched with films of nuclear emulsion, i.e., in a high-accuracy tracking device assembled according to the ECC principle. The detector (Fig. 9a), with a mass of about 1.25×10^3 t (of which nearly 100 t fell on the nuclear emulsion) and size of $20 \times 10 \times 10$ m, provided many statistics necessary for recording ν_τ with the interaction cross section of 10^{-37} cm^2/nucleon at energies of about 20 GeV. The detector was a hybrid facility of two identical super modules, including a target and a muon spectrometer. Each target consisted of 2920 blocks (bricks), assembled according to the principle of an ECC chamber, alternating with horizontal and vertical planes of target tracker (TT) scintillators. The TTs were used for target designation to select the bricks in which the neutrino interaction could occur. Each brick, with a mass of 8.3 kg, consisted of 57 emulsion films, alternating with 56 lead plates 1 mm thick and having an area of 12.7×10.2 cm. The thickness of one brick corresponded approximately to ten cascade units (c.u.), which provided the development of an electromagnetic shower within the brick. The target structure allowed extracting any brick from it, if necessary. A light-proof packet with two emulsion challenge sheets (CSs) was attached to the back wall of a brick. The use of CS doublets allowed checking the occurrence of neutrino interaction in a particular brick. The correctness of the brick choice was confirmed if at least one track compatible with those reconstructed in electron detectors was found in the CS films. The detection efficiency with this procedure of selecting one most probable brick or, if necessary, two most probable bricks amounted to 77%. When from two to three bricks per event were processed, the analysis efficiency reached 83%.

The total area of emulsion films mounted in the target modules amounted to 110,000 m^2 and the area of the lead plates was 105,000 m^2. During the entire time of the experiment in the underground LNGS laboratory using the robotized assembling method, about 150,000 bricks were fabricated with the use of more than nine million emulsion films.

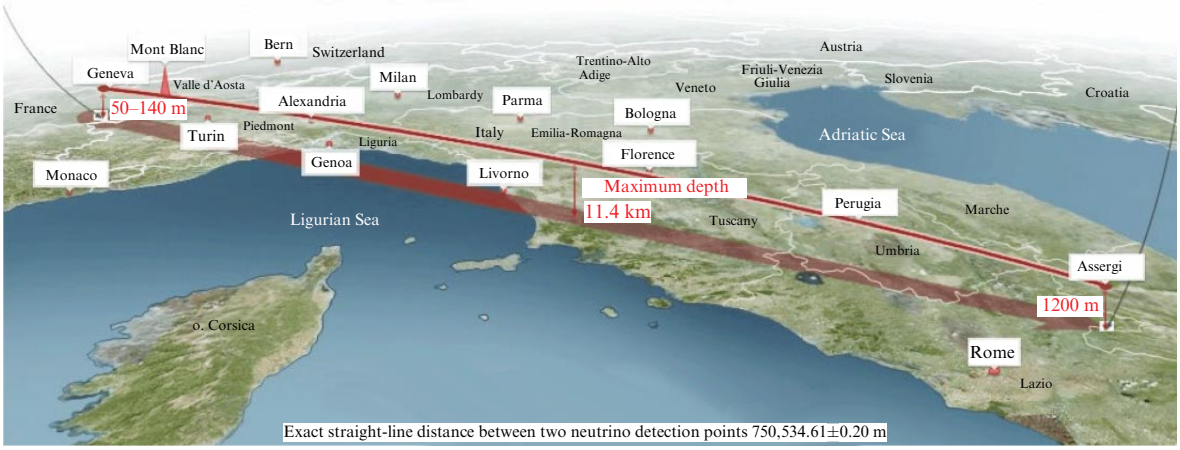

Figure 8. Schematic of neutrino beam's passage from CERN to LNGS.

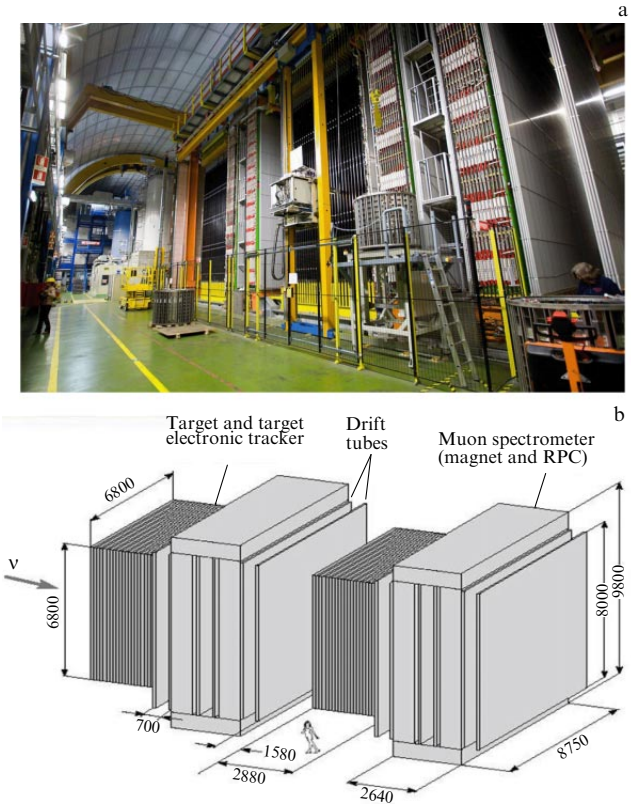

Figure 9. OPERA detector in LNGS underground laboratory: (a) general view of detector; (b) schematic diagram of detector. Dimensions are in cm.

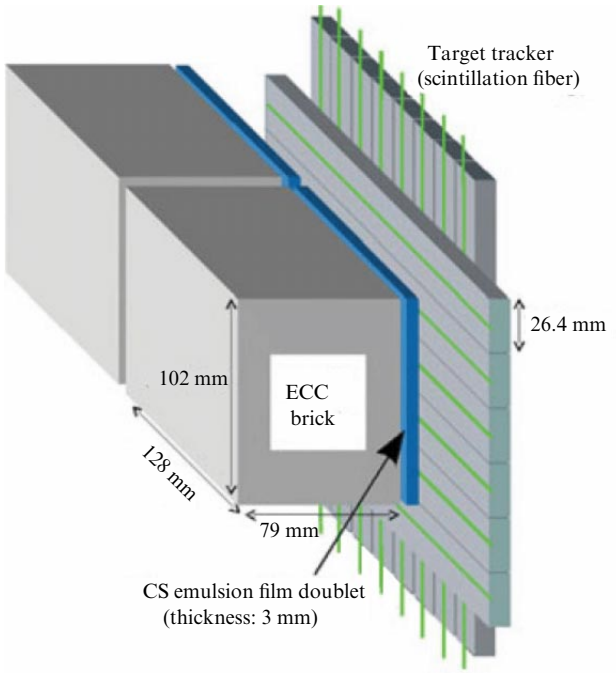

Figure 10. Schematic of mounting bricks in target [5].

Behind each of two target supermodules, a magnetic muon spectrometer was located. The core of each magnet consisted of 12 plates of iron 50 mm thick, alternating with gas resistive plate chamber (RPC) detectors and high-resolution drift tubes (Fig. 9b).

Neutrino interactions were recorded in nuclear emulsions with submicron spatial resolution. The principle of the experiment can be formulated as follows. Initially, the products of neutrino interactions were recorded by TT scintillators, placed behind each wall of the target (Fig. 10). The 'shower axis' reconstruction or registration of the track of a penetrating particle (e.g., a muon) allowed identifying the brick in which the interaction could occur. This brick was extracted from the wall, the attached doublet of CS emulsion films was taken off and developed, while the brick, still being packed, was placed in the underground store waiting for the results of scanning the changeable layers. Bricks that were incorrectly identified by scintillation trackers as containing interactions were not dismantled but returned to the target with a new CS packet, avoiding unnecessary processing and scanning of falsely identified bricks. So, the CS doublets performed the two most important functions in the experiment: confirming the fact that a brick contained neutrino interaction and recording the tracks of charged particles from this interaction for inverse ECC scanning (see below).

When one or several tracks related to an event in a CS were detected, the selected brick was exposed to cosmic rays for 12 hours to obtain a set of reference tracks for precise topological and kinematical measurements. Then, the brick was dismantled, and its films were developed. The tracks found in the CS served as the basis for the so-called procedure of inverse scanning, which consisted of tracing the track in emulsion films of the brick, starting from the brick's back wall to its disappearance. The track disappearance indicated a possible vertex of neutrino interaction.

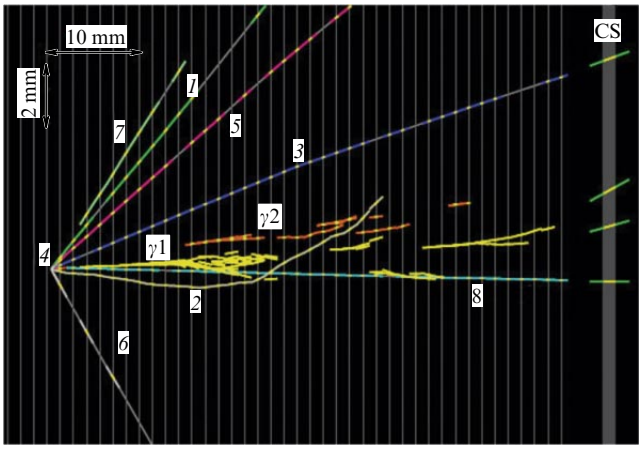

Figure 11. Reconstruction of first interaction of tau neutrino in OPERA experiment [29].

Within the region with a volume of about 1 cm^3 around the point of track disappearance, using a special technique [28], the scanning of emulsions was performed, aimed at detecting partner tracks and/or secondary interactions. This procedure was applied to find charmed hadrons that were created in the tau neutrino interactions.

Thus, to find the candidate events for neutrino interactions in the OPERA experiment, a thorough kinematic analysis was performed by measuring the energy of the electromagnetic cascade developed in the ECC unit, determining the momenta of the charged particles by measuring multiple Coulomb scattering in the brick, and tracing the tracks in the subsequent walls of the target. During the experiment, more than 25 thousand interactions of all types of neutrinos were recorded.

The scanning of events was carried out in 12 laboratories of several countries by means of 40 automated microscopes. At the universities of Salerno and Napoli (Italy), special software was developed for primary data processing, in the creation of which LEP LPI researchers took part.

In the process of online scanning with automated microscopes, registration was carried out of the so-called micro-tracks of particles passing through each sensitive layer of an emulsion plate. 'Sewing' two micro-tracks in one film through a plastic substrate, implemented using specially designed software, allowed reconstructing in this film a part of the trajectory of the particle, called the base track. To reconstruct tracks of particles in the entire volume of the target, the base tracks in subsequent films were united using a Calman filter.

The first candidate for a tau neutrino was recorded in 2010 [29]; the event reconstruction is presented in Fig. 11. It is seen that the interaction is caused by neither a muon nor an electron. The primary vertex contains seven tracks, one of which has the topology of a kink decay. From the kinematic analysis carried out, it follows that the observed decay corresponds to the channel $\tau \to \rho\nu_\tau$ followed by the decay $\rho \to \pi^0\pi$. In the period from 2012 to 2015, four more events with ν_τ were recorded [30]. The scanning of emulsion films was completed in 2016.

During the experiment from 2008 to 2012, statistics of 1.8×10^{20} protons per detector target were accumulated. The result was the discovery of muon to tau neutrino oscillations with a statistical significance of 6.1σ based on the observation of ten ν_τ under interaction through the charged current channel. The registration of muon to tau neutrino oscillations in the OPERA experiment entered the scientific substantiation of the Nobel Prize in Physics of 2015. The data of the experiment are published on the open data CERN portal.

2.1.4 SND@LHC experiment. At present, LEP staff members are working in the international collaboration of a new experiment called the Scattering Neutrino Detector at LHC (SND@LHC) at CERN [31]. This is a compact autonomous experiment for recording all three neutrino flavors and searching for weakly interacting particles at LHC, which at present is carrying out measurements in the earlier unexplored pseudorapidity range of $7.2 < \eta < 8.6$. The detector is also capable of recording particles of light dark matter scattered by target atoms in the range of parameters supplementary to the experiments already being carried out. The CND@LHC experiment was proposed in 2020 and prepared for launch in December 2021. Already in 2022, the first data were obtained. The facility is located in the TI18 LHC tunnel 480 m from the IP1 point of the collision of counterpropagating beams in the ATLAS detector. The detector is a hybrid system based on a target of tungsten plates interleaved with emulsion and electronic trackers, behind which the muon system is located. Such a configuration allows distinguishing neutrinos of all three flavors in the range of energies unavailable for other experiments at LHC. The use of nuclear emulsion allows searching for weakly interacting particles in the detector target.

An intense narrow collimated (within polar angles of < 2.5 mrad) beam of neutrinos with energies from 100 GeV to a few TeV, created in the interactions of protons with an energy of 13.6 TeV in the center-of-mass frame, passed through the detector, located quite close to the accelerator beam axis. High energy neutrinos arise in lepton W and Z decays and the decays of hadrons, incorporating b and c quarks. Thus, the neutrinos in the studied pseudorapidity region from 7.2 to 8.6 can be considered an indicator of the creation of heavy flavors. The neutrino flavor is determined by the type of appropriate charged lepton and the decay kinematics. In particular, tau leptons are identified by the observation of a characteristic tau decay vertex in the emulsion and by the absence of an electron or muon in the primary vertex.

The SND@LHC detector (Fig. 12) was designed so that at limited dimensions it could provide (a) a sufficient amount of matter to measure the energy of the particles in the calorimeter and high efficiency of muon identification; (b) the transverse dimension of the target, allowing the registration of particles in the required pseudorapidity interval.

The neutrino target implemented according to the ECC technology is used as a vertex detector, which, due to high resolution in nuclear emulsion, allows identifying τ leptons and charmed hadrons, disentangling their production and decay vertices. The electrons are identified by electromagnetic showers formed in the target. The neutrino target consists of five emulsion blocks (walls) installed in parallel with a transverse dimension of 384×384 mm and total weight of 830 kg. Each wall is composed by four cells (bricks) of 60 emulsion films alternating with 59 tungsten plates 1 mm thick. The parameters of one wall are shown in Fig. 13a. The entire neutrino target contains 1200 emulsion films with a total area of about 44 m^2.

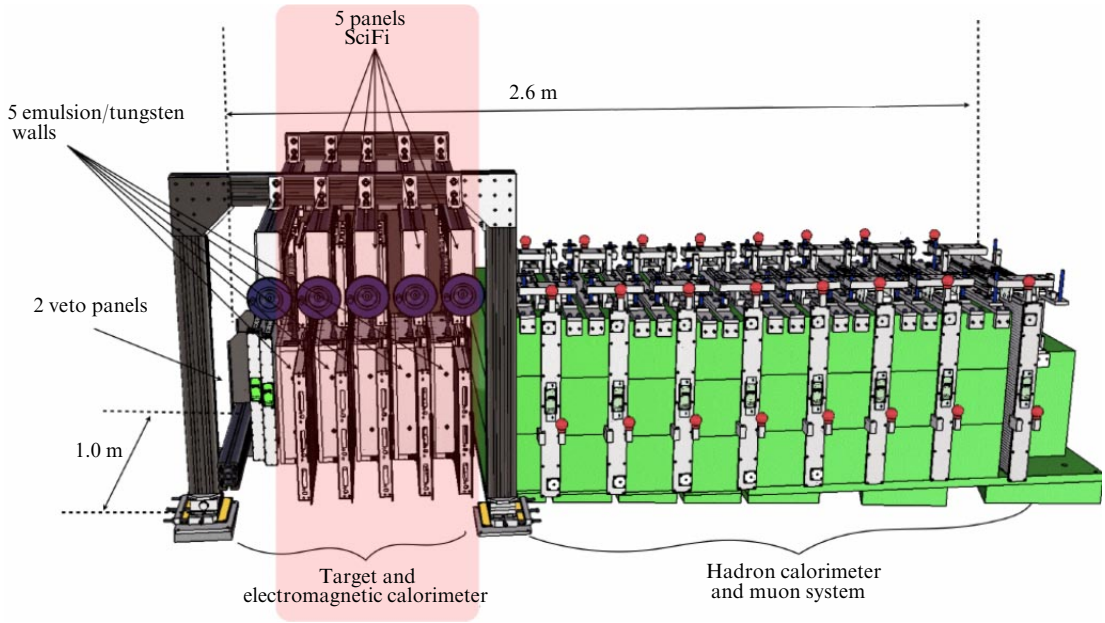

Figure 12. Schematic image of SND@LHC detector. Neutrino target is color highlighted.

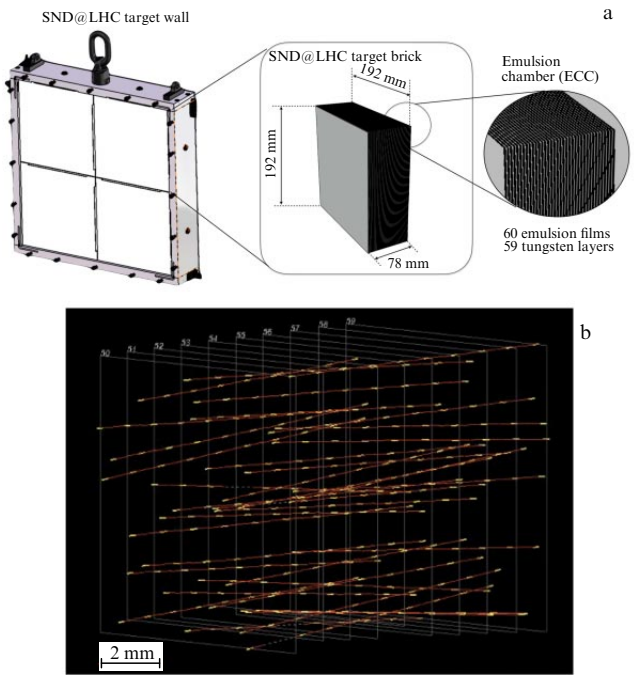

Figure 13. Neutrino target of SHD@LHC experiment: (a) schematic of one wall of target; (b) result of track reconstruction in ten consecutive films of one brick. Yellow segments denote base tracks (data from SND@LHC experiment [32]).

A detector made of SciFi scintillation fibers is placed behind each of the five walls of the target. The use of SciFi allows localizing the position of neutrino interaction in the emulsion block and relating the muon track reconstructed in the emulsion to the track recorded by the muon detector, located behind the neutrino target. The muon identification system consists of iron plates, alternating with detectors of scintillation rods. The combination of SciFi and the scintillators of the muon detector (the hadron calorimeter) serves also to measure the energy of the hadron jet arising in neutrino interactions and, therefore, the energy of a neutrino. The total length of the detector amounts to nearly $11\,\lambda_{\text{int}}$, which ensured proper development of hadron showers.

The development of the exposed emulsions of the neutrino target is carried out in the CERN chemical laboratory, equipped with the necessary instrumentation for processing 1200 emulsion films per week. The viewing of the developed emulsions is performed using optical microscopes of five specialized scanning laboratories, as a result of which the experimental data processing time is comparable to the exposure time. The scanning was performed in the laboratories of the universities of Bologna and Napoli, the University of Zurich, the Lebedev Physical Institute of RAS (LEP), as well as the recently created CERN laboratory. The rate of emulsion processing with automated optical microscopes reaches ~ 180 cm^2 h^{-1}.

The event reconstruction is performed in two stages. At the first stage, the target designation data from electron detectors are processed. Then, the emulsion data are analyzed, which become available after scanning the nuclear emulsion films for nearly half a year after their irradiation by the beam. The algorithm of reconstructing events in nuclear emulsions is analogous to that developed for the OPERA experiment (Fig. 13b).

According to estimates, emulsions allow analyzing the images of reconstruct events at a maximal density of tracks to 10^7 cm^{-2}; however, at such high density, the track tracing in the target is accompanied by serious technical difficulties. As a result, an irradiation level of the order of 10^5 tracks cm^{-2} is considered optimal. Therefore, considering the estimated background in TI18, the emulsion exposure in one session of irradiation should not exceed 30 fb^{-1}, which means replacing the emulsion bricks nearly three times a year under the continuous operation of the accelerator (1 fb^{-1} corresponds to about 7×10^{13} pp interactions).

To date, six exposures of the emulsion target have been implemented (Emulsion RUN0–RUN5). The first exposure was aimed at testing the construction and quality of the neutrino detector assemblage; therefore, it had the smallest load of 0.5 fb^{-1}. During the second and subsequent exposures, the target in full assemblage was irradiated:

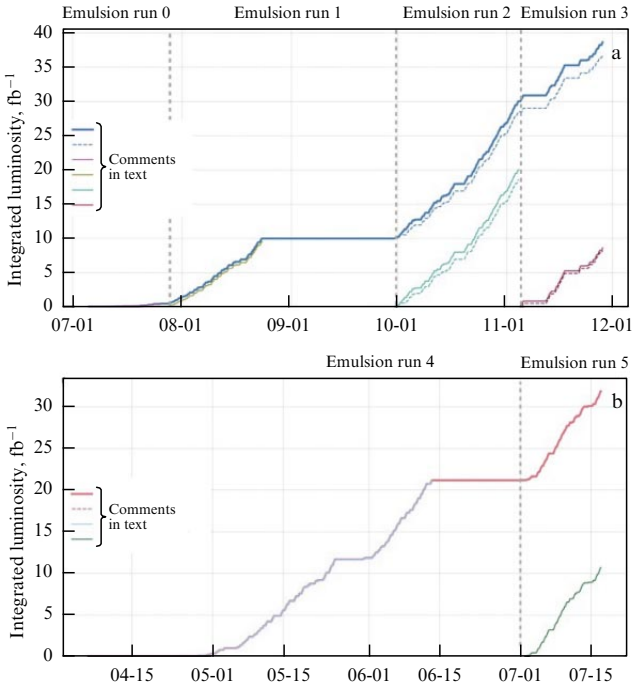

Figure 14. Integrated luminosity reflecting the number of interactions collected per irradiation session for periods (a) 2022 and (b) 2023; *x*-axis shows dates of sessions by year.

5 walls with 4 bricks, each containing 60 emulsion layers, which makes 1200 emulsions per session. Starting from the third exposure, the neutrino detector recorded data synchronously with electronic detectors (the dashed lines in Fig. 14).

The diagrams in Fig. 14 show the acquirement of intensity in the sessions RUN0–RUN5, where bold solid lines indicate that the emulsion target was subjected to the beam action.

Filling the neutrino detector with emulsion layers in each exposure and the acquired integrated luminosity are presented in Table 1, where the symbols N and S denote the emulsion producer (N for the University of Nagoya, Japan; S for the LHC Torgovyi Dom Slavich, Russia). The monitoring of the quality of the Russian emulsion before the delivery to CERN was carried out by LEP staff members.

Table 1. Technical characteristics of neutrino detector assemblage and RUN1–RUN5 exposures.

RUN ID	Number of bricks and layers of neutrino detector	Integrated luminosity, fb^{-1}
RUN0	1 brick = 57 N	1.5
RUN1	20 bricks = 513 N + 660 S	9.5
RUN2	20 bricks = 1140 N	20.0
RUN3	20 bricks = 886 N + 266 S	8.6
RUN4	20 bricks = 1140 N	21.2
RUN5	20 bricks = 1140 N	10.7

From the data presented in Table 1, it is seen that some of the sessions (RUN1, RUN3, RUN5) had a cumulative integrated luminosity of ~ 10 fb^{-1}, which corresponds to an integrated intensity of the order of $10^4 - 10^5$ racks cm^{-2}. When increasing the integrated luminosity to 20–30 fb^{-1}, the filling reaches $\sim 10^5$–10^6 tracks cm^{-2}, which requires upgrading the algorithm of track reconstruction. At present, intense work is being performed on upgrading the track reconstruction algorithm, which, among other things, will increase the speed of processing emulsion data without changing the constituent scanning stations.

At present, the detector position with respect to the beam line corresponds to the schematic diagram in Fig. 15a. However, in 2024, it is planned to change the detector position, placing it symmetrically with respect to the beam axis, as shown in Fig. 15b.

Such a shift will lead to higher energies of the neutrinos (200–400 GeV), which in turn will increase by more than four times the yield statistics of electron and muon neutrinos (Fig. 16). In this case, the studies will shift to the region of pseudorapidity $\eta > 7.4$.

To date, the SND@LHC experiment is in the stage of active data collection. The processing of emulsion data is carried out simultaneously in laboratories in several countries involved in the collaboration. Along with the processing of the experiment results, the modeling of the response of each detector component is performed using the DPMJET-III [34] and Pythia8 + FLUKA software packages [35]; the development and testing of the system of data collection and

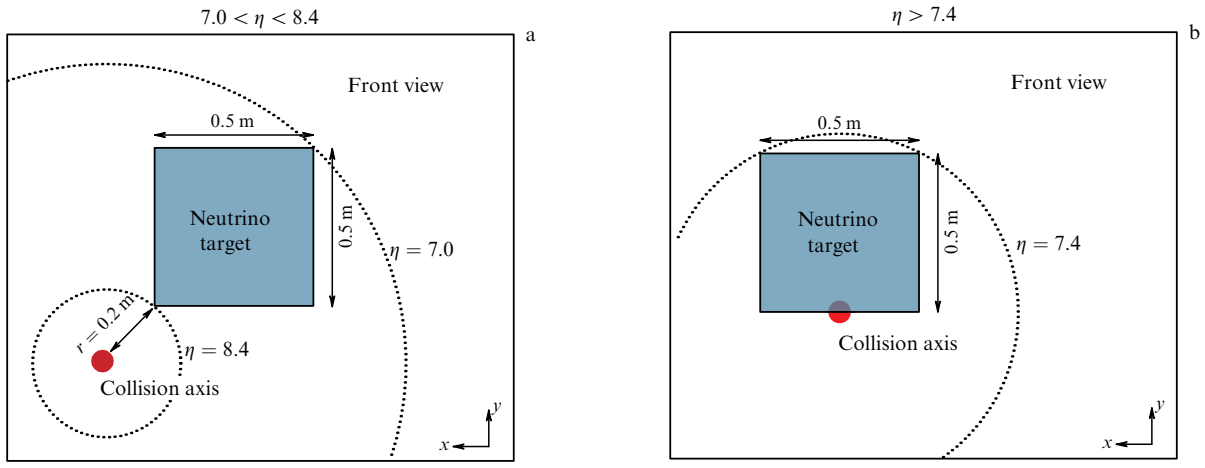

Figure 15. Schematic representation of SND@LHC neutrino detector relative to beam axis, front view; (a) during exposures RUN1–RUN5, (b) expected position for subsequent exposures [33].

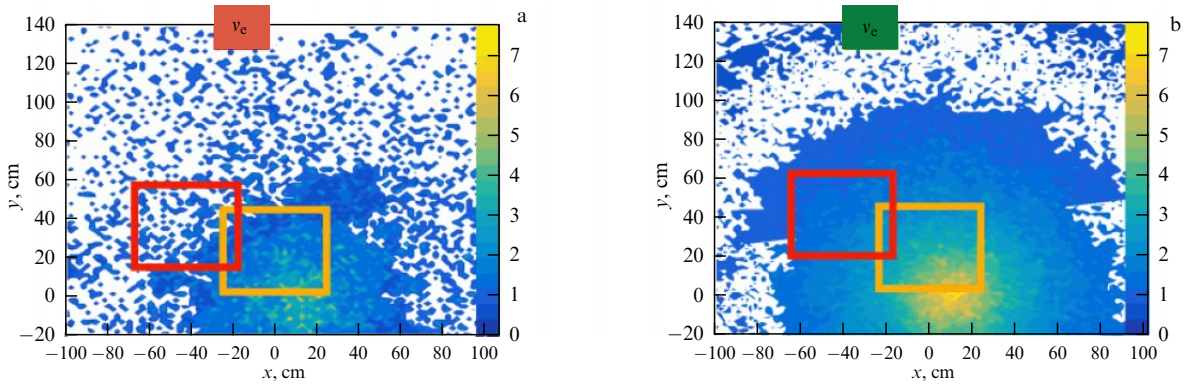

Figure 16. Schematic representation of SND@LHC neutrino detector relative to beam axis, front view. Color scale shows expected number of interactions ν_e and ν_μ for (a) RUN1–RUN5 exposures, (b) subsequent exposures [33]. Red square highlights investigated pseudorapidity region $7.0 < \eta < 8.4$, yellow square, region $\eta > 7.4$, corresponding to planned shift of the detector to a new position relative to beam axis.

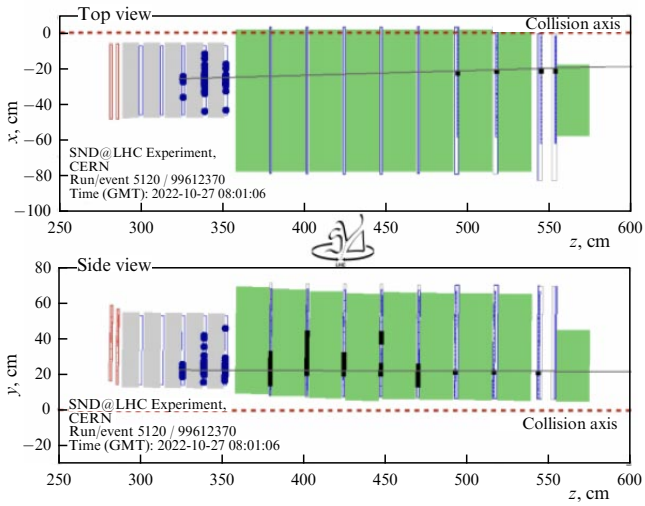

Figure 17. Neutrino interactions through ν_μ CC charged current in SND@LHC neutrino detector. Signals from SciFi and hadron calorimeter are shown as blue and black dots, respectively. Black line represents reconstructed track of produced muon in the muon detector [36].

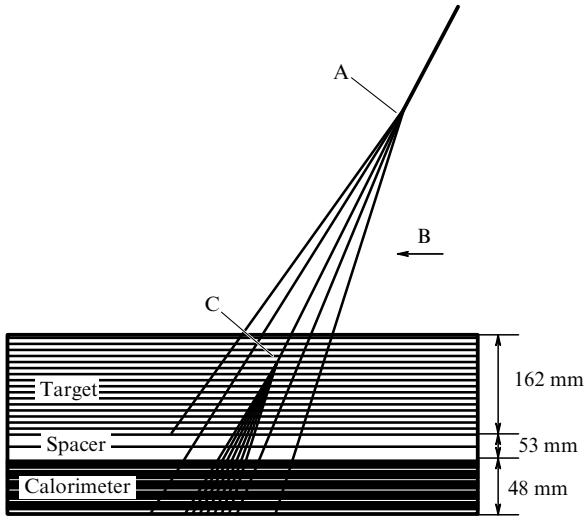

Figure 18. Schematic representation of STRANA gamma-hadron family in X-ray emulsion chamber: A — interaction of a primary cosmic ray particle in atmosphere above the chamber; B — shower development before entering the chamber; C — secondary interaction of leading particle in target block of the chamber.

information storage at one of the CERN servers is being carried out. Subsequent exposures of the neutrino detector in the range of pseudorapidity $\eta > 7.4$ and energy 200–400 GeV will allow increasing the yield of ν_e and ν_μ interactions by more than four times.

In 2022, the first neutrino oscillation event upon the collision of protons was recorded at the LHC. The scheme of signal development representing this event with the electronic part of the SND@LHC neutrino detector is presented in Fig. 17. In the SND@LHC experiment, eight candidates for events with the formation of muon neutrinos ν_μ in the charged current (CC) channel, recorded by the electronic devices of the detector, were selected. The statistical significance of the selected events amounted to nearly seven standard deviations. At present, the analysis of emulsion data (scanning of emulsion plates, track reconstruction, physical analysis) of the RUN1–RUN5 exposures is being executed.

The first results of the SND@LHC experiment obtained in 2022 are published in [36], indicating the prospects of further studies in the poorly explored region of neutrino energies from 350 GeV to 10 TeV and being of great interest for investigating neutrino anomalies in a material with high statistical support.

2.2 Track technique in astrophysics

2.2.1 X-ray emulsion cameras on balloons, STRANA event. One of the first LEP experiments using emulsion technology was the balloon experiments based on X-ray emulsion chambers (XECs) for studying cosmic radiation in the upper layers of the atmosphere.

Before the appearance of high-power accelerators, XEC facilities were widely used in cosmic ray experiments to study energy and charge spectra and specific features of the interaction of high energy particles (see [37–39]). The XECs used at LEP consisted of the target part, assembled according to emulsion cloud chamber (ECC) technology [37] from layers of nuclear emulsion alternating with layers of absorber, and the bottom part (calorimeter), where, in addition to layers of nuclear emulsion, X-ray films were located, sandwiched with lead plates 0.5 cm thick, which practically corresponds to the radiation length of this material. Darkenings in the X-ray film served to target events and estimate the energy of the particle that caused the shower. To spatially separate the shower particles, the target part and the calorimeter were separated by a ‘spatial block’ (Fig. 18). The analysis of the events recorded in the XEC was based on the

reconstruction of tracks of all charged particles created due to interactions in the passive material of the facility. In nuclear emulsions, the angular characteristics of the segments of each track outgoing from the vertex were measured and the reconstruction of the hadron shower in the volume of the of the XEC target part was implemented.

In the LEP experiments of 1970–1980, X-ray emulsion chambers were exposed in the upper atmosphere at an altitude of more than 30 km (atmospheric residual layer of about 10.2 g cm^{-2}). Chambers with an area of 40×50 cm were installed on balloons that flew from Kamchatka to the Volga region. The total weight of the useful load of each balloon was about 2 t.

The most interesting result of these experiments was recording the unique gamma-hadron family STRANA, caused by nuclear interaction in the atmosphere directly above the chamber. Because of the limited chamber depth, the recording efficiency of hadrons at the facility amounted to about 40%. Nearly 30% of the produced particles were lost because the event developed nearer to the chamber edge. Taking these corrections into account, the total energy of the family was evaluated to be approximately equal to $(1-2) \times 10^{16}$ eV. It should be noted that such energies are still inaccessible with accelerators.

As a result of interaction of the primary cosmic radiation particle, whose trajectory slope to the normal was about 30°, 107 particles were created, of which 76 were identified as γ quanta with a total energy of more than 1400 TeV; the total energy of 30 particles identified as hadrons amounted to about 2500 TeV (without the leading particle) [40]. The leading particle of the hadron cascade with an energy of $(1-2) \times 10^{15}$ eV experienced one more interaction in the carbon absorber of the target unit of the chamber, and the tracks of the charged particles of the formed jet were observed in the lower-lying layers of the nuclear emulsion (Fig. 19a). Its electromagnetic component produced a large darkening region (halo) in the X-ray film of the calorimeter (Fig. 19b) (the chamber calorimeter thickness was nine cascade units). The fact that no particle track has been found in the 12 upper layers of the XEC before the interaction in the target unit testifies to the leading particle not being heavier than the He nucleus. The data obtained in nuclear emulsions of the target unit by counting the number of tracks per area unit allowed finding the spatial distribution of tracks in the jet.

The interaction altitude was estimated by three different methods: by reducing pairs of gamma quanta to the hypothetical point of origin, by analyzing the pseudorapidity distribution of particles in the family, and by the triangulation method using the minor difference between the coordinates of spots and tracks formed by particles when passing through the chamber in different recording layers. In the latter case, the measurement of coordinates of spots from electromagnetic showers was carried out by a computer program using the images in the X-ray films scanned with an optical device. The tracks in nuclear emulsions were measured on semiautomated microscopes at LEP. A total of about 800 tracks and spots were measured (Fig. 20); only the cascades found in more than two layers of the calorimeter were used in the calculations.

Different methods of altitude estimation yielded a discrepancy in the interval from 50 to 1200 m. Such a considerable discrepancy is explained by the large measurement error caused, in particular, by the errors in coordinate referencing of nuclear emulsion and X-ray layers in the calorimeter, in the thicknesses of the lead plates, and the deviation in the superfamily characteristics from the mean estimation values. Thus, it was shown in [43] that the local fluctuations in the distortion of the nuclear emulsion can substantially increase the errors in such a delicate procedure as triangulation.

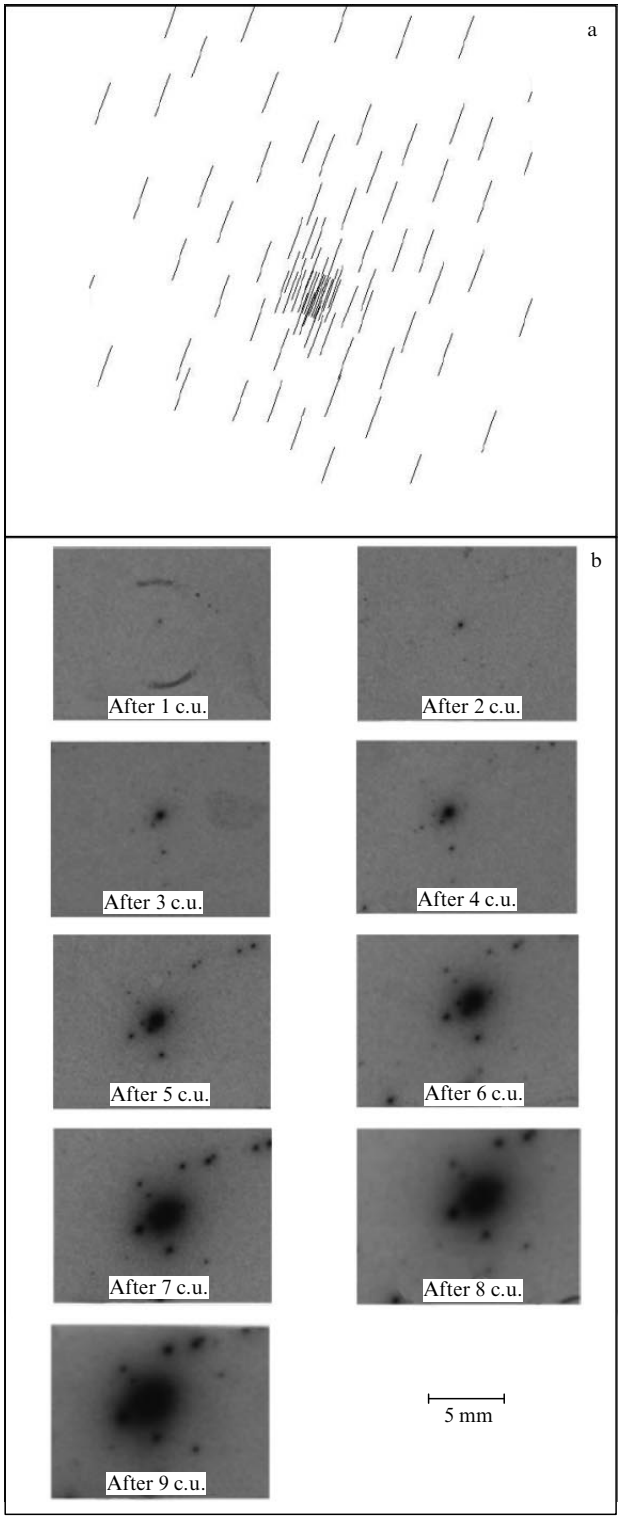

Figure 19. (a) Jet in one layer of nuclear emulsion of XEC target block; (b) development of jet halo in XEC calorimeter [41].

The determination of the interaction altitude allowed estimating the transverse momenta of the particles created in

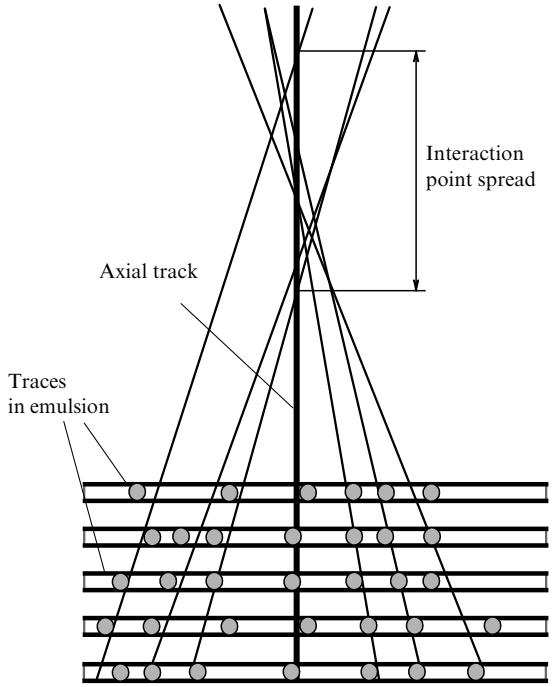

Figure 20. Schematic diagram illustrating cascade triangulation method in the XEC calorimeter [42].

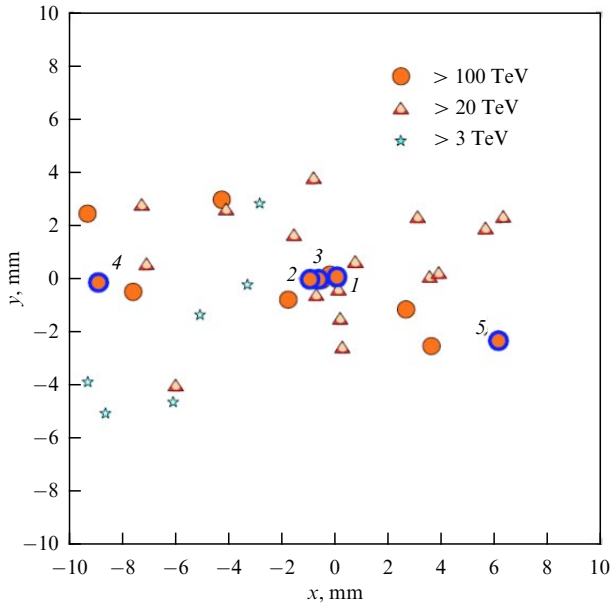

Figure 21. Target diagram of central part of STRANA superfamily. Five highest-energy hadrons are designated by numbers [43].

the primary interaction. According to the estimates, the value of the mean transverse momentum [43] in the superfamily exceeded 2.5 GeV s^{-1}, and, for the most probable altitude of interaction of $\sim$ 300 m, could amount to about 10 GeV s^{-1}. The type of primary nucleus was determined as CNO.

In the STRANA superfamily, the phenomenon of alignment was observed, which manifested itself in the fact that, in the calorimeter, the spots of darkening with the highest energy were 'aligned' with minor deviations along a straight line in the plane perpendicular to the trajectory of the primary particle. This effect is a consequence of the coplanar scattering of secondary particles upon nuclear interaction with an energy higher than 10^{15} eV, when the highest-energy objects in the gamma-hadron families align along a straight line [44]. In the STRANA superfamily, 15 of 107 particles were located near the alignment line (Fig. 21); these 15 particles took away more than a half of the energy of the particle that caused the primary interaction. In addition, expressed anisotropy was observed in the location of all particles in the central zone of the family. The direction of elongation of the anisotropic distribution of particles coincided with the direction of alignment of the five hadrons with the highest energy, i.e., during the expansion, these secondary particles were distributed near the plane of coplanar expansion. Estimates were obtained according to which the probability of a random event with such a degree of alignment is from 0.001 to 0.03% for different nuclei [40].

The STRANA superfamily occupies a special place among the results ever obtained in any balloon experiment for several reasons. First, it is necessary to note that approximately one cosmic particle with an energy of 10^{15} eV or higher is incident on 1 m^2 of the boundary of the terrestrial atmosphere in a year. Considering that nearly 85% of these particles are protons, the probability of detecting a heavier particle with this energy with a small-area setup tends to zero. The recorded superfamily is also remarkable for the fact that the leading particle caused a secondary interaction in the 12th layer of the target XEC unit. The halo phenomenon earlier observed only in experiments with broad atmospheric showers in the mountains was first observed in the hadron interaction, detected at stratospheric altitude. Finally, while such high energies of interaction of nuclei of the CNO group cannot be reached with accelerators, the STRANA family became the first case of observing the alignment effect earlier observed only in experiments with broad atmospheric showers (see, e.g., [45]).

2.2.2 Searching for superheavy nuclei in olivine crystals from meteorites. One of the most significant experiments performed at LEP during the last 20 years was OLIMPIA (abbreviation of the Russian for Olivines from Meteorites — Search for Heavy and Superheavy Nuclei) devoted to the search for tracks of nuclei of cosmic origin in olivine crystals from pallasites, initiated by Academician V L Ginzburg and supported by Academician Yu Ts Oganessian [46]. The subject of study was olivines — fragments of the iron-stone meteorites (pallasites) Marjalahti and Eagle Station, used as track detectors.

The search for heavy elements in the composition of galactic cosmic rays (GCRs) is extremely difficult because of the small fluxes of these nuclei in the circumterrestrial space ($\sim 1-2$ particles per m^2 in a year, i.e., more than 10 orders of magnitude weaker than the flux of hydrogen nuclei). Therefore, in multiple experiments on detecting the nuclei of cosmic radiation using balloons [47] and satellites [48–51], only a few ten tracks of nuclei with the charge $Z > 86$ and a few individual events identified by the authors of studies as tracks of nuclei with $Z > 92$ were found. For this reason, pallasites as detectors of superheavy nuclei possess an undoubted advantage, namely, an unprecedented duration in space. In particular, the radiation age of Marjalahti and Eagle Station meteorites could be from 30 to more than 200 million years [52] (the radiation or cosmic age of a meteorite coincides with the duration of its exposure to cosmic rays and is counted from the moment of expulsion of the meteorite as a separate

Figure 22. Fragments of pallasites Marjalahti (*1*) and Eagle Station (*2*) used in OLIMPIA experiment.

cosmic body). As shown by estimates [53], during 10^8 years of exposure in cosmic space, 1 cm^3 of the meteorite matter at a depth of 5 cm from its preatmospheric surface can contain 10^2-10^3 tracks of nuclei with $Z > 90$, and at a depth less than 1 cm, up to 10^4 such tracks.

Pallasites consist of porous nickel-iron matrices with inclusions of olivine crystals (Fig. 22). Olivine (chemical formula $(Mg_{0.8}Fe_{0.2})_2SiO_4$) is a semitransparent mineral, whose crystals with dimensions from a few millimeters to 1–2 cm can occupy up to 65% of the meteorite volume. The olivine crystals possess specific features that allow using them as track detectors. First, they can preserve during hundreds of millions of years the structural and phase changes in the crystal structure caused by the passage of a fast heavy ion. Second, under the influence of laboratory chemical agents, due to the significant excess of the rate of dissolution of the material in the track area over the rate of dissolution of the undamaged material, the resulting defects in the crystal lattice increase in size so much that they become visible in an optical microscope. The transparency of the crystals allows observing in visible light the tracks 'developed' by chemical etching. Finally, due to a sufficiently high threshold of specific energy losses of a charged particle, necessary to form in the olivine a chemically etchable track (more than 18 MeV mg^{-1} cm^2 [54]), the tracks of nuclei with charges $Z \leqslant 24$ are completely absent in the olivine, which allows studying the charge composition of cosmic rays in the region of heavy nuclei starting from Fe, without a background effect.

In Russia, studies of olivines from pallasites aimed at searching for traces of heavy cosmic nuclei were initiated in the Laboratory of Nuclear Reactions of the Joint Institute for Nuclear Research (LNR JINR) [55], and, in the early 2000s, fragments of the Marjalahti and Eagle Station pallasites were passed to LEP LPI in order to explore them at the PAVICOM-2 facility (see Section 4). The olivine crystals used in the OLIMPIA experiment were at a depth of no more than 5–6 cm from preatmospheric surface of the meteorites, i.e., at a depth where it is possible to find nuclei with energies of $\sim 1.5-5$ GeV per nucleon [56].

For the convenience of processing, the olivine crystals extracted from the iron-nickel matrix were fixed in 10×20-mm epoxy tablets. In such a form, the crystals were subjected to grinding, polishing, etching, and measurements with a microscope (Fig. 23).

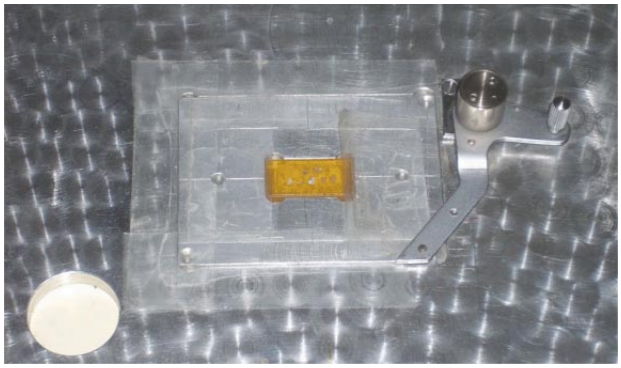

Figure 23. Epoxy tablet with olivine crystals fixed on the object table of the PAVICOM-2 microscope.

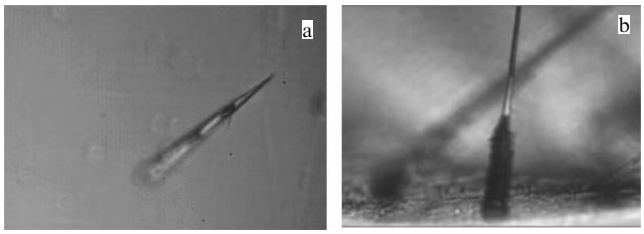

Figure 24. Micrograph of tracks of superheavy cosmic ray nuclei etched in olivine crystals from pallasites: (a) 'carrot,' (b) 'syringe.' Size of field of view in micrographs is $(60-100) \times 140$ μm.

The microphotographs of the heavy nuclei tracks in the olivine with a magnification of up to 60$^\times$ are shown in Fig. 24. Depending on the ionization losses, the etched tracks-channels of high-energy heavy nuclei can look like a 'carrot' (a) or, in 2% of cases, a 'syringe' (b) (consisting of two parts, a cylindrical one before the stop and a needle-like one at the trajectory segment, corresponding to higher energy of the particle, forming a syringe-shaped structure, the diameters of the channels of one track differing by several times).

The measurement and data analysis technique developed at LEP, which is substantially different from the methods used at LNR JINR, was based on determining the parameters of the etched tracks of nucleus deceleration before their stop in the olivine [57]. The main methodological problem of the experiment was to determine the charge of the nucleus that formed the track. The charge evaluation was carried out using the results of measuring the parameters of the etched track. In addition to the geometric characteristic, the measured length L of the etched track segment, one more dynamic characteristic was used, namely, the etching rate $V_{\rm etch}$ along the track. The necessity of introducing an additional parameter was due to the fact that the etched length of a track could exceed the crystal size.

To ensure the most accurate determination of the parameters of the nucleus tracks and the efficient use of the crystal volume, the OLIMPIA experiment used a method of successive step-by-step cutting-etching of the surface layers of the crystal. During measurements in the next layer, a procedure of 'sewing' it to the previous cut layer was carried out, during which a search for the continuation of the tracks was carried out. On completion of crystal processing, the total track length was summed considering the track slope angle to the surface. The etching rate was determined at each stage of the processing. Comparing the etching rate values of the

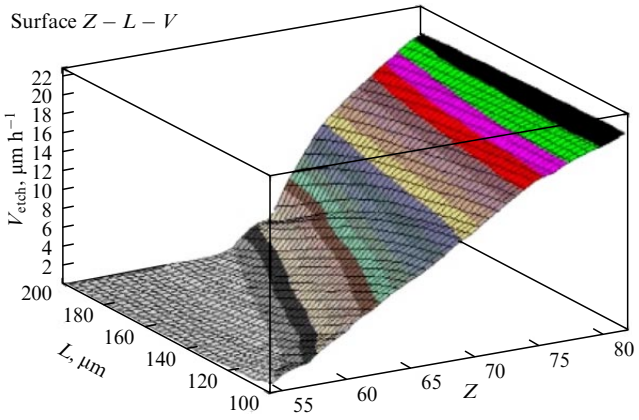

Figure 25. Calibration surface for determining charge of nucleus z from measured path length L and track etching rate V_{etch}.

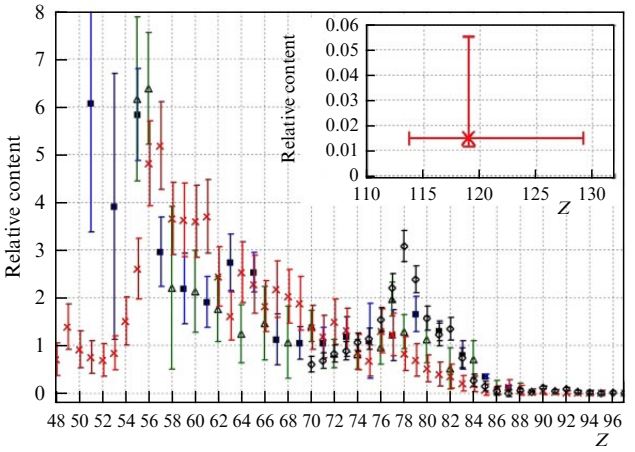

Figure 26. Relative content of heavy GCR nuclei recorded in OLIMPIA experiment (X's, with statistical errors) in comparison with the results of other experiments: ARIEL-6 (triangles) [48], HEAO-3 (squares) [49], and UHCRE (diamonds) [51]. Inset shows three transfermium nuclei recorded in this work.

tracks measured at sequential stages of processing ensured a high accuracy of measuring the track parameters used in the identification of nuclear charges.

To obtain a quantitative relation between the etching rate V_{etch} and the measured free path length of a nucleus before its stop L, calibrating experiments were performed in accelerators with the nuclei of various elements [58]. Based on the results of the calibration experiments, the three-dimensional function $Z(L, V_{etch})$ was constructed for determining charges of the nuclei, recorded in the meteorite olivine (Fig. 25). The method of estimating the charge value consisted in two-dimensional interpolation of the surface using the measured values of V_{etch} and L for the etched track. The accuracy of charge determination according to this method depends on the position of points on the plane and ranges from ± 1 to ± 2 charge units. To determine large charges $67 < Z < 93$, the calibration curves, relating the etched length, the etching rate, and the charge, were approximated by a five-parameter function, which allowed extrapolating the dependence of the charge of heavy nuclei by several units beyond the limits of the calibration experiments to the region $Z > 92$.

The authors' method of layer-wise grinding and etching of crystals, in combination with a procedure to process them at PAVICOM, allowed collecting vast material for analysis. During the experiment, 853 crystals of meteorite olivine were collected, in which it was possible to identify 25,851 tracks of cosmic origin with charges $Z > 40$, including 2771 nuclei with $40 < Z < 50$, 22,617 nuclei with $50 < Z < 80$, 457 nuclei with $80 < Z < 92$, and 6 nuclei with $92 < Z < 100$. The data in the region of charges $Z < 56$ are less significant statistically, since, due to the small lengths of such tracks, their measurement was difficult.

The charge spectrum of nuclei with $Z \geqslant 48$ is presented in Fig. 26 in comparison with the results of most significant satellite experiments on recording heavy nuclei in circumterrestrial space [59]. The data are normalized by the content of iron nuclei ^{26}Fe (10^6).

In Figure 26, it is possible to notice discrepancies between the results of the OLIMPIA experiment and satellite experiments. In this connection, it is worth noting that in the satellite experiments the fluxes of nuclei in the circumterrestrial space are registered, whereas in the meteorite substance fluctuations of nuclear fluxes can be fixed, produced in such global events as supernova explosions, the merging of neutron stars, or the merging of a neutron star and a black hole, occurring in the relative proximity of the meteorite during its travel in deep cosmic space. It was shown in [60] that noticeably exceeding the relative flux of superheavy nuclei as recorded in meteorites, in contrast to satellite experiments, can mean an additional contribution of such nuclei. Since these events occur at different times and at different distances from the Sun, the contributions of various classes of events to the local flux of cosmic nuclei continuously vary, forming the temporal history of charge spectra of heavy components of the local flux. Understanding this history will allow formulating substantiated conclusions about the history of various nucleosynthesis events in the vicinity of the Solar System and, therefore, about the mechanisms of nuclear synthesis in the Galaxy.

An illustration of this effect is the difference in the number of nuclei of one group, recorded by means of meteorites with different radiation ages, which is a direct indication of the effect of particles created in local cosmic processes and accompanied by the expelling of such nuclei. Taking into account that such cosmic events as a supernova explosion or merging of neutron stars are rare, to realize the scenario described above, the experimental data on the history of GCR fluxes should contain information about the nuclei accumulated over hundreds of millions of years. Therefore, it is essential that the OLIMPIA experiment explore two meteorites with different radiation ages: Marjalahti (according to different estimates, from 178 to 205 million years) and Eagle Station (from 35 to 71 million years). The difference between the spectra of nuclei found in these two meteorites can be explained by the fact that the time between two cosmic events (from 140 to 170 million years), accompanied by the release of heavy nuclei, exceeds the exposure age of the 'younger' meteorite and is less than the exposure age of the 'elder' one. A comparison of the superheavy nucleus spectra recorded in different meteorites, as well as by satellite detectors, can help us to understand the short-term history of fluxes of heavy and superheavy nuclei affecting the Solar System. The results of the OLIMPIA experiment show that, during the last 200 million years, the Solar System could at least twice have been irradiated by fluxes of nuclei from the events of cosmic nucleosynthesis, as a result of which very large yields of the heaviest elements were created [61].

In 2013, participants in the OLIMPIA experiment reported the detection of tracks in the meteorite substance of particles whose charges were estimated to lie in the interval from 103 to 129 [58], which can be considered the first direct evidence of the existence of stable superheavy nuclei of natural origin. The length of the corresponding tracks amounted to more than 500 μm, and the etching rate V_{etch} exceeded 35 μm h^{-1}. Since the maximal experimentally measured value of the track etching velocity for uranium nuclei in olivine before their stop is 26 ± 1 μm h^{-1}, this result means that the charges of the detected nuclei substantially exceed the charge of the uranium nucleus. An estimate of this charge by regression analysis yielded the value of 119^{+10}_{-6} with a probability of 95%.

The detected superheavy nuclei obviously had to live long enough to fly from the place of their formation to the surface of the meteorite, i.e., their lifetime should be at least comparable to the time of their propagation from the source to the asteroid belt of the Solar System, from which most meteorites arrive at Earth. Estimates show that the minimal lifetime should be from 50 to 100 years, which is many orders of magnitude longer than the lifetime of transfermium nuclei synthesized in accelerators. Therefore, the detection of such nuclei can testify to the existence of a 'stability island' of superheavy nuclei.

3. Modeling processes of track formation using fast heavy ions in solid-state track detectors

Describing the mechanisms of formation of structurally modified regions as a result of irradiation of solid-state detectors by fast heavy ions (FHIs, $M > 20$ a.u.m., $E > 0.1$ MeV per nucleon) requires considering the main features of the track kinetics. The realization of different relaxation channels of the excited track region leading to structural changes substantially depends on the values of parameters characterizing the initial excited state of the material in this region. Quantitative determination of these parameters, depending on the characteristics of the incident ion and irradiated material, is a matter of principle for the interpretation of the experiment results.

A heavy nucleus in the detector material becomes an ion, since it acquires an equilibrium charge [62]. The characteristic damage of the atomic structure of a target stimulated by FHIs has a transverse dimension (diameter) from 1 to 10 nm [62, 63] and can be observed only either in a transmission electron microscope or by means of X-ray diffraction at the target. Such studies require high radiation doses (from 10^{10} ions per cm^2), and the sample should be destroyed to study the tracks along the trajectory. Therefore, the overwhelming majority of track techniques are based on chemical etching of the FHI tracks. In a chemically active medium (as a rule, a liquid etching agent), the rate of dissolving the damaged atomic structure around the ion trajectory is higher than the rate of dissolving undamaged material beyond this region. As a result of FHI track etching, hollow channels of micrometer size are formed, which can be observed and measured with an optical microscope.

As early as 1967, it was noted that the track length in the target and the etching rate along the track depend on the type of ion and its energy [64]. This effect was used in subsequent experiments on identifying nuclei of cosmic radiation in plastic detectors on satellites [51] and nuclei of cosmic radiation in the meteorite substance [60, 65, 66]; the etching of tracks from fission fragments was used for geochronological analysis [67, 68]. The controlled irradiation in accelerators and the subsequent etching are used to synthesize nanostructures, nanowires, nanopores, and high purity filters [69, 70].

The nanosized modification of materials using FHIs allows creating regions with changed electronic properties [71], including ensembles of quantum dots in nanoelectronics. [72]. Ion therapy is applied in medicine to treat oncological diseases [73], e.g., for elimination of inoperable brain tumors [74].

One of the main issues associated with heavy ion irradiation is radiation safety. Cosmic rays are a danger for space flights [75]: high-energy ions break bonds in DNA [76] and water, producing chemically active fragments and free radicals that interact with genetic material [77], which can damage the DNA up to a lethal dose [76, 77]. The passage of FHIs leads to program failures and damage to elements in computing hardware [78]. Long FHI exposure can lead to macroscopic damage of materials, which should be taken into account when using nuclear materials and handling nuclear waste [79]. The key problem for these studies remains the possibility of comparing the parameters of the projectile nucleus (heavy ion) with the results of the destruction of the target material and subsequent etching, i.e., calibration.

For most of the trajectory along which the detected track arises, the incident heavy ions have an energy $E > 0.1$ MeV per nucleon and are decelerated, exciting the electron subsystem of a condensed target [80]. The maximum of electron losses per unit length of the trajectory (the Bragg peak, Fig. 27) is reached at the incident ion velocity approximately equal to the velocity of atomic electrons [80]. For heavy ions (Au, Bi, U), the electron losses in the region of this peak reach values of 40–50 keV per nanometer of trajectory. Electron losses of energy become less than elastic losses at ion energies below ~ 1 keV per nucleon.

The investigation of the kinetics of FHI track formation is also of considerable fundamental interest [62]. The FHI track kinetics start from a state in which the electronic subsystem of the material in the nanometric vicinity of the ion trajectory reaches extreme excitation levels, while the atomic system remains unperturbed. This state of material exists for a very short time (~ 1 fs) and is not observed with any other kind of impact. The kinetics of exciting the lattice of the material due to its interaction with the relaxing electronic subsystem in an FHI track is characterized by ~ 10 nm and 10–100 fs spatiotemporal scales. These scales are so small and the excitation intensity is so large that the macroscopic models based on the assumption of local equilibrium become poorly applicable.

The experimental and theoretical activity in this field sharply increased in the 1990s, when the development of experimental techniques gave an impetus to the development of nanotechnologies based on exposure to FHIs [63]. Up to 2010–2015, at least four classes of models were formulated using semiempirical rules of choosing the FHI parameters for particular purposes. Recent review [62] thoroughly discusses the insufficient fundamental substantiation of the approximations used and the lack of predictive power of these models: the Coulomb explosion [83], the exciton model [84, 85], the model based on the propagation of shock waves [86], and various versions of the thermal burst model [87, 88]. Their common drawback is the lack of predictive power caused by the use of fitting parameters.

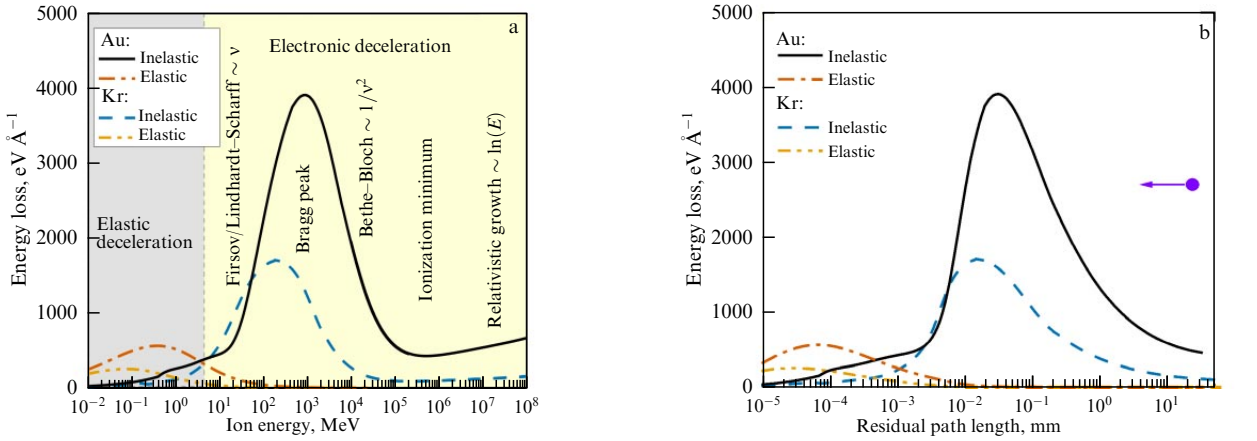

Figure 27. Elastic and inelastic energy losses of Au and Kr ions in Al_2O_3, calculated using SRIM code [80] for nonrelativistic and TREKIS code [81, 82] for relativistic energies, depending on (a) the energy of the incident ion or (b) the residual range of the particle (direction of ion penetration is shown by the arrow).

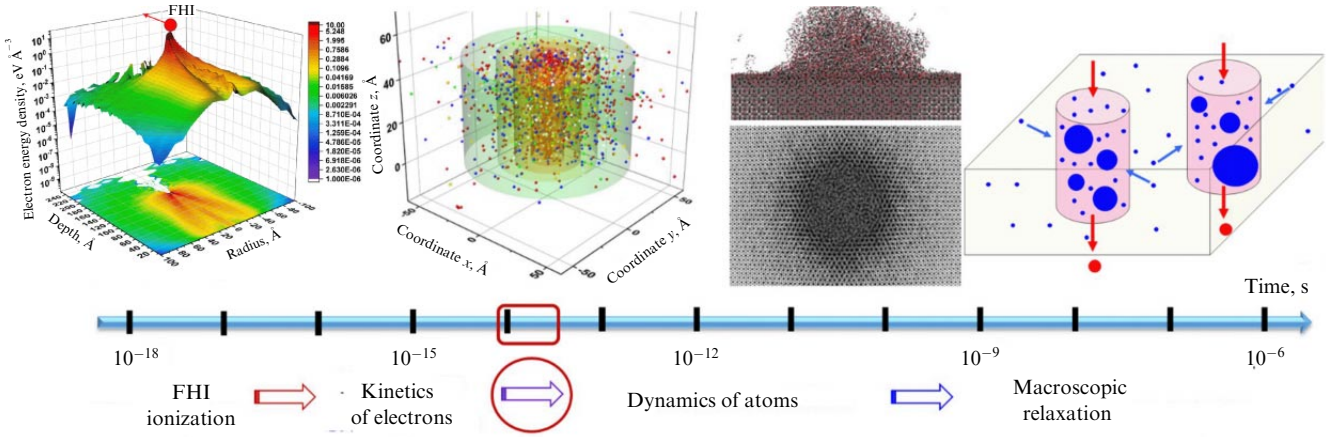

Figure 28. Schematic illustration of characteristic time scales of kinetics and FHI track origin.

The problem of describing the FHI track kinetics can be solved considering their multiscale nature. The processes initiated by ion passage cover more than ten orders of magnitude in time (Fig. 28). For different processes involved in track creation at different intervals of this time scale, several modeling methods are available, suitable for a quantitative description of each stage of track formation with the required accuracy. However, to date, there has been no self-consistent model capable of implementing the most appropriate approach at each time interval and ensuring a consistent connection between these stages while considering the entire time interval of track kinetics with good accuracy.

This possibility was first successfully implemented in the model which was developed during the last decade with the active participation of LEP LPI [89–91]. The idea of the model is based on the fact that, due to the fast cooling of the electronic subsystem, its dynamics are separated in time from the dynamics of the atomic ensemble. At times after the ion passage of less than $\sim$ 100 fs, the original Monte Carlo (MC) code TREKIS [89] is used, describing the interaction of the incident FHI with the target and the excitation and relaxation of the electron subsystem, as well as exciting the target atomic system by transferring some of the electron excitation energy to it.

The distribution of energy transferred to the atomic ensemble from the electronic subsystem was used as the initial condition. Such an approach ensures proper overlap and information exchange between the model blocks and preserves the required level of accuracy during the entire modeling process. In this case, molecular dynamic modeling is performed on time scales from $\sim$ 100 fs to $\sim$ 100 ps of the atomic subsystem response to the introduced excitation and formation of the observed structurally modified FHI tracks. The principal feature of the model is using special sections in the MC code that allow for the collective reaction of the electron and ion subsystems of the material to the introduced excitation, as well as the 'nonthermal' mechanism of energy transfer to the ionic subsystem as a result of acceleration of atoms, initiated by a sharp change in the interatomic potential of a solid-state target as a result of extreme excitation of its electron subsystem [92].

The constructed model using no fitting parameters can predict the track parameters for various ions, which is a fundamental achievement in the problem of describing the effects of material irradiation by FHI beams. The application of the model allowed for the first time a description of track formation 'from beginning to end' without using fit parameters and in good agreement with experiment. The model has been multiply tested in studies carried out by various research teams (see, e.g., [62, 93]).

As to the track etching technique, the application of the model made it possible for the first time to determine quantitatively the parameters and morphology of structurally modified regions along the trajectories of various ions in

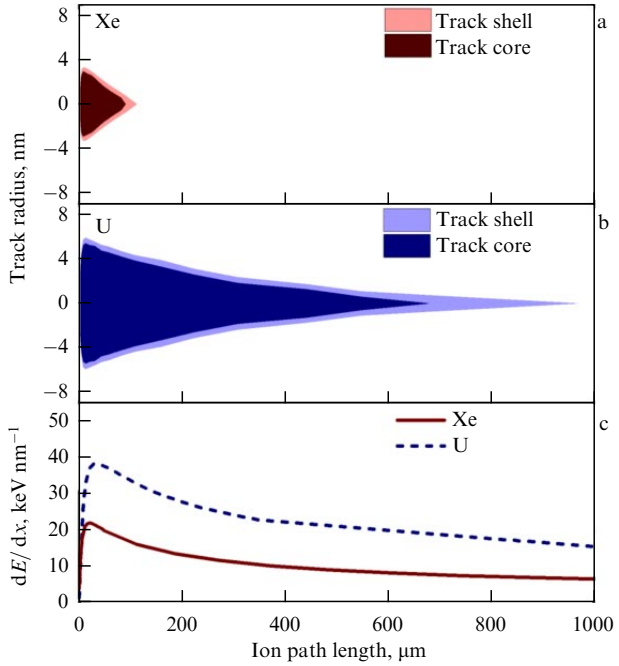

Figure 29. Track regions depending on position on trajectory for (a) Xe (length of 104 μm) and (b) U (length of 978 μm) ions in olivine [94]. For comparison, Fig. c shows dependences for electron energy losses of ions.

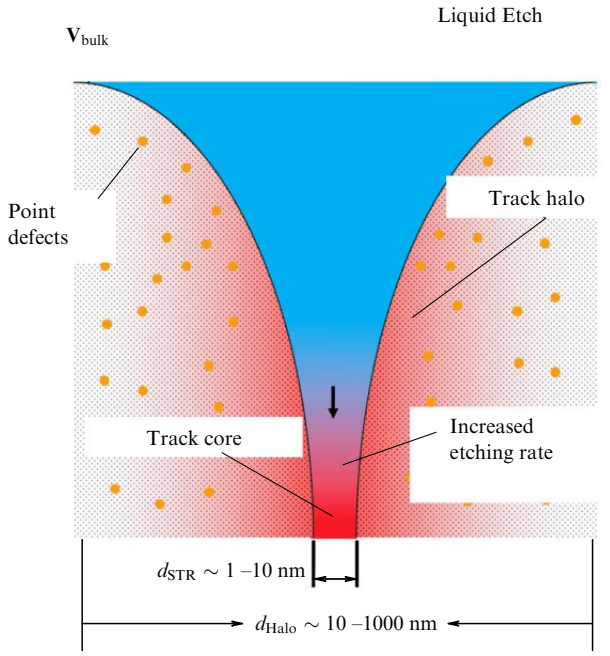

Figure 31. Illustration of model of liquid etching of FHI tracks in olivine [96].

the meteorite olivine [94]. Figure 29 shows the amorphized region, the track core, and the region of the track transit to the crystalline matrix (cladding).

For comparison, Fig. 30 presents the curves of electronic energy loss. It is seen that the position of the loss peak at the ion trajectory (Bragg peak) does not coincide with the region of maximal structural damage. For example, for Xe ions, the maximal radius of the damaged region is observed at an energy of ~ 130 MeV, which significantly differs from the energy ~ 500 MeV, corresponding to the Bragg peak. The maximum damage caused by U ions occurs at much lower energies (~ 250 MeV) than the Bragg peak position (~ 1000 MeV). This fact indicates the universality of disagreement: the maximum energy loss of ions does not lead to maximum damage of the material. When decelerating a high-energy FHI, the maximum damage occurs at a larger depth along the ion trajectory than that at which the Bragg peak of electron losses of the ion energy arises (Fig. 30a). This effect is associated with the difference in the spectra of electrons generated by 'slow' and 'fast' ions and is important for experiments and applications of ion irradiation and for ion therapy [95].

Using the information on the character and specific features of structural modifications as a baseline, it was possible to construct a model of olivine chemical activation along the trajectory of the incident FHI [95] and formulate an original model of liquid etching of FHI tracks in this material [96, 97] (see illustration in Fig. 31). It is important that the model use no fit parameters, which is of fundamental significance for the calibration procedure of the track technique, requiring an unambiguous relation between the parameters of the projectile ion and those of the etched region.

The model was tested using the results of calibration experiments carried out in the laboratories GSI (Darmstadt, Germany) and IMP (Lanzhou, China) within the framework of the OLIMPIA experiment [57]. A comparison of the results of modeling with the experimental data is presented in Fig. 32.

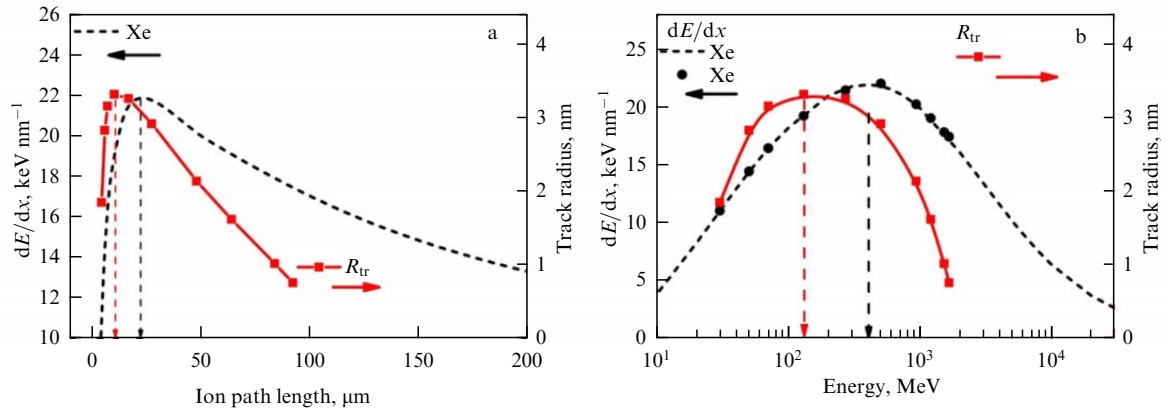

Figure 30. Track sizes and electron energy losses of Xe ion as functions of (a) the ion path and (b) the ion energy [93]. Vertical arrows indicate positions of maxima on corresponding curves.

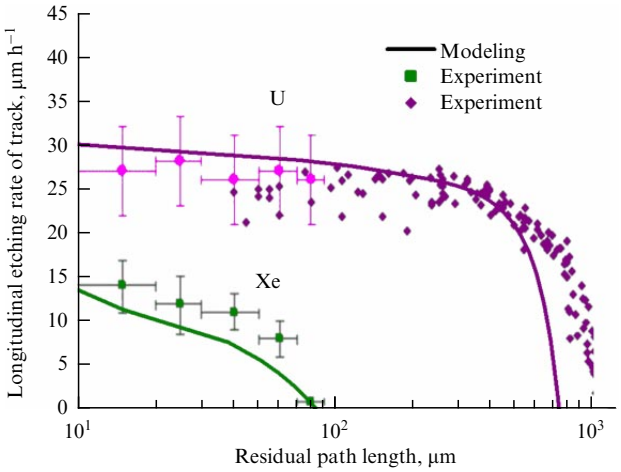

Figure 32. Dependences of etching rate along tracks on residual path length based on results of calibration experiments [57, 58] and results of using the multiscale etching model [97].

The modeling carried out allowed calibrating the technique developed at LEP to determine the charges of the incident heavy nuclei from the composition of GCR by the parameters of their etched tracks in the meteorite olivine. A natural continuation of this work was describing olivine etching at the atomic level using an original atomistic model, which has predicted the formation of nanopores with a noncircular transverse section under olivine etching [98].

4. Up-to-date methods of processing and analysis of track detector data

Efficient processing of ever-growing volumes of data is possible provided that new methods of image analysis in track detectors are being developed. A new stage in the development of track detector technology is related to achievements in the field of scanning systems, aimed at increasing the efficiency and rate of data processing, first of all, at the expense of introducing automated methods of autonomous analysis based on fast electronics and mechanized object tables with a high accuracy of translation.

In the late 1990s and early 2000s, the PAVICOM automated optical measuring complex was created at the Lebedev Physical Institute of the Russian Academy of Sciences specifically for the EMU-15 experiment (see Section 2.1.2) for high-tech processing of experimental data in the field of nuclear physics, cosmic ray physics, and high-energy physics obtained using track detectors [99, 100]. Using PAVICOM, the search and digitation of tracks of charged particles in the detector material, recognition and tracing of the tracks, and systematization and primary data processing are performed in a fully automated mode.

The main feature of PAVICOM that distinguishes it from similar scanning systems in other laboratories of the world is its independence of the type of processed data. Consisting of three independent measuring setups, the complex allows processing the data of track detectors of various types (nuclear emulsion, plastic detectors, phosphate glasses, olivine crystals from meteorites, etc.). PAVICOM setups mainly differ by the dimension of the subject tables, which determines the range of translation of the optical system in the plane of the detector and, correspondingly, the admissible size of materials to be processed.

The operating mode of the PAVICOM complex satisfies a number of strict requirements for the measuring system, including the ability to continuously scan and process images in real time, the ability to quickly adapt to new equipment, efficient operation in multiprocessor systems, and inclusion in distributed computing. The software is based on a modular approach, which provides the necessary flexibility in setting up the system and allows scanning various types of detectors.

In 2021–2022, the complex was substantially upgraded, facilitating an increase in the scanning rate and the efficiency of data processing by increasing the resolution power and image capture rate. The upgrade allowed confirming the status of the PAVICOM setups as universal for Russia and corresponding to the best world-class examples [101]. The instrumentation for PAVICOM microscopes was completed with the following components: Mikrotron EoSens4CXP video camera (monochrome, with a C-Mount lens), CXP 5W5 DIN1.0/2.3 to DIN1.0/2.3 video camera cable 5 m long with a microEnable 5 ironman AQ8-CXP6D image capture board, Nikon CF1 Plan Fluor 20X MI lens, 20x, graphics station (iRU Corp 719 TWR i9 9900K PC//64 gb/4 + 4TB 7.2k/SSD512GB/RTX2080ti 11GB/NVINDIA GeForce RTX 2080Ti/W10Pr64), PT-121-RAX-L15-MPH LEDs (Luminus Devices), EA-PS 3040-20 programmable power supply, and more.

The largest PAVICOM-1 facility comprises a large high-precision table (MICOS) with the optical system, equipped in accordance with the experimental task. It includes a massive platform and a movable subject table with the dimensions of 500×800 mm (Fig. 33). Above the table, the optical unit, equipped with the Mikrotron EoSens 4CXP C-mount video camera with the possibility of translating in the vertical plane, is attached. The accuracy of positioning the subject table with respect to the microscope is 0.5 μm. The table vibration stability is ensured by the large mass of the setup ($\sim$ 1 t). To reduce the thermal expansion, the holder for mounting the microscope is made of granite. The subject table is controlled both from a computer and by joystick in the manual mode. The control of the system instrumentation and data processing online is implemented by modern computers included in the equipment of each microscope.

The Mikrotron EoSens 4CXP C-mount video camera is a device based on the monochrome CMOS digital matrix with a resolution of 2336×1728 pixels and a maximum rate of 563 frames per second. In the optical scheme, the Nikon CFI Plan Fluor 20X MI objective lens is used, having a numerical aperture of 0.75 and providing a magnification of $20^{\times}$. The analog signal from the video camera is transmitted through the special CXP5W5 data cable to the input of the SiliconSoftware microEnable-5 image capture board, the technical characteristics of which are compatible with the parameters of the camera and graphic station. This configuration was designed in a collaboration between LEP LPI and Instituto Nazionale di Fisica Nucleare, Italy [102].

One more facility of the complex, PAVICOM-2 (Fig. 34), adapted to operating with crystals and optical glasses, was designed based on the LOMO MPE-11 microscope with an integrated precision table (Carl Zeiss, Germany), combined with a control unit. The microscope optics project the object image on the CMOS camera with a magnification of up to $90^{\times}$.

The translation of the PAVICOM optical table in all coordinates is implemented by step motors manipulated by a

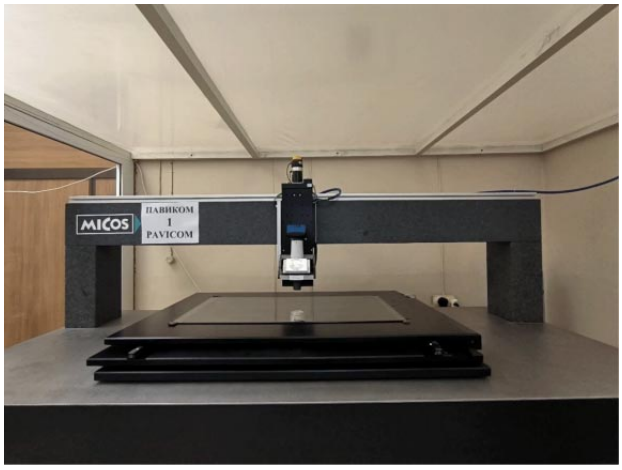

Figure 33. PAVICOM-1 setup.

Figure 34. PAVICOM-2 setup.

Carl Zeiss controller, to which the commands are delivered from a computer. The accuracy of measurement of the x, y, and z coordinates is 0.25 μm. The limits of automated translation of the table along the x-axis are from 0 to 120 mm and, along the y-axis, from 0 to 100 mm; the objective can move along the z-coordinate within 10 mm.

The PAVICOM-3 setup (Fig. 35) was mainly used to scan the nuclear emulsions of the OPERA experiment. The motorized object table of the PAVICOM-3 microscope is analogous to that of PAVICOM-1, but has a smaller range of translation (200 × 200 mm). The vacuum system for fixing the emulsion on the object table in the process of scanning supports a pressure within the limits of 250–500 mbar. The PAVICOM/LASSO program [103] controlling the movement of the scanning station is installed on a computer connected via a controller to the table mechanics.

Simultaneously with the table movement, the graphic station processes the images from the Mikrotron EoSen4CXP camera, connected to it through the microEnable5 image capture board. The GPU board with CUDA technologies used for the initial processing consists of several flow SMP multiprocessors and allows considerable acceleration of the obtained data analysis. In the process of upgrading the system, a program module was developed and implemented that allows the units to exchange large data arrays with

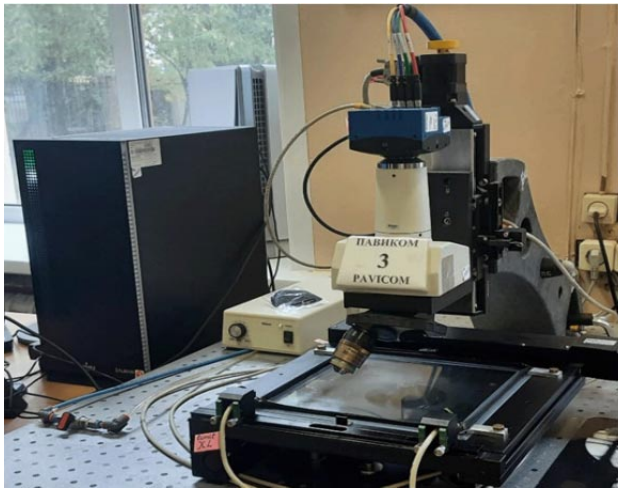

Figure 35. PAVICOM-3 setup.

high speed and reliability. The module ensured data transmission through TCI/IP networks, allowed controlling the transmitted data integrity, and demonstrated reliable operation in the system, using a common network with a data transfer rate of 1 Gbit s^{-1}. The huge volume of processed data requires several computers for complex analysis. For the primary identification of a track in the offline mode after the upgrade, a separate computer is used with software based on the FEDRA program complex [104]. The result of upgrading the PAVICOM system was an increase in the scanning velocity up to the modern world standard of 190 cm^2 h^{-1}.

PAVICOM was used to process the data from such experiments as EMU-15, OPERA, and OLIMPIA, mentioned above, and to process and analyze the data from the SND@LHC experiment and muonographic studies of cultural heritage objects on the territory of Russia [105, 106]. Such a gigantic data volume requires innovative methods of image analysis that ensure rapid and high-quality processing of experimental data at a fundamentally new level. The wide development of image recognition techniques led to designing new algorithms for image processing.

At the initial stage of image processing in nuclear emulsions, the dark regions corresponding to processed grains of silver are selected (so-called segmentation). For this procedure, the preliminary processing of images is used that includes filtering, binarization, etc. (see [26]). The members of the PAVICOM team (LEP LPI) implemented the segmentation of images in nuclear emulsions for the first time by means of a neural network (U-Net architecture), which makes it possible to reveal both global and local specific features of the images [107]. The advantages of using this network for image segmentation are the open-source code and the flexibility of the system, which allows the code to be adapted to any analytical tasks without the need to create the network from scratch.

U-Net, like any neural learning network, requires an 'initial image–segmented image set.' The training process consists of choosing such parameters of the network at which it executes the task of segmentation best. On PAVICOM-3, a training sample of 1261 initial images, each 1280 × 1224 pixels in size and the same number of ethalon segmented images obtained by the standard method, were prepared.

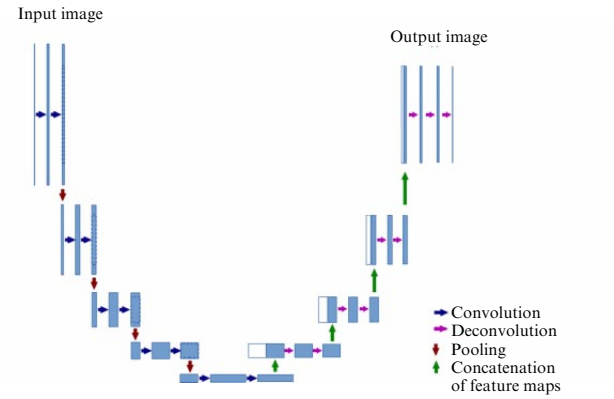

Figure 36. Architecture of U-Net convolutional neural network [107].

The U-Net architecture consists of two paths: contracting (convolution) and expanding (pooling), which form a U-shaped structure (Fig. 36). This allows efficient extraction of the information on the content of the image at different levels of hierarchy and then using this information for precise segmentation of objects.

At the first processing stage, the initial images arriving at the input of the contracting path of the neural network (the left-hand side of Fig. 36) undergo the following transformations. First, in each pixel of the image and its vicinity, a convolution is performed with numerical matrices (cores) with dimensions of 3×3 or 5×5, the pixel sequence of which reflects a certain feature (line, angle, spot, etc.). The resulting convolutional images are transformed by overlapping a mask (a 2×2 matrix), which moves over the image. Inside each matrix position, the number is determined (usually, the max-pooling number), which becomes an element of a new matrix. The obtained matrix forms a feature map. As a result of this procedure, the dimensions of feature maps become half the size of those of convolutional images, and the features studied are amplified. The procedure of convolution and feature mapping multiply repeats, leading to a step-by-step reduction in the map dimensions. At each step, the number of feature maps increases.

The next stage is an inverse process, the expansion of the obtained feature maps of the initial image (the right-hand side of Fig. 36), which is executed using numerical matrices with the same number of steps as in the convolution. In this case, the feature maps at each step are concatenated, their number decreases, and the dimension grows (up convolution). At the end of the procedure, only one matrix is left. As a result, the initial image is transformed into a segmented one. It is compared to the reference segmented image, prepared for training.

An important aspect of training a neural network with U-Net architecture is the choice of the loss function, which determines how accurately the segmentation performed by the network matches the reference sample. In application to image processing in nuclear emulsions, the binary focal cross entropy most optimal for problems of binary classification [108] was used as the loss function. After comparing the transformed initial and reference images, corrections to the network parameters are calculated by the method of reverse error propagation. For this purpose, the method of gradient descent is used.

The stages of image processing by a neural network are determined by epochs, each of which includes the processing of all samples. After each training epoch, the output image is compared with the delivered reference segmented image and the Jaccard similarity coefficient is calculated, characterizing the proportion of the area of correctly marked clusters. The Jaccard coefficient is defined as the ratio of the intersection area (logical 'AND') and the union area (logical 'OR'). The closer its value to one, the more precise the network selects the clusters belonging to the signal. At the beginning of the procedure, with the growing number of epochs, the degree of coincidence of segmented images obtained by the network and the reference images increases. However, after a certain number of epochs, the result of the network operation stops improving and can even worsen (so-called overtraining, one of the problems of deep learning neural networks). For this case, an algorithm has been implemented that chooses the best result of the present epochs.

Table 2. Program code modules for the U-Net neural network and their functions.

Module name	Module functions
Import all libraries	Connect Python libraries for extracting data from cloud storage, processing it, displaying it on the screen, and adding it to the training set, as well as libraries required for creating and training a neural network
Extracting files from storage and converting them	Extracting, processing, and converting source images to the required format
Image Data Generator	Creating a generator that generates similar images based on known images
Creating a neural network and training it (saving the best result)	Building a convolutional neural network and training it over several epochs
Training results	Displaying several example images from the training set and an image generated by the neural network (indicating the Jaccard coefficient)
Saving the model	Loading large volumes of numerical, graphic, and text data into one file (extension *.h5)
Loading the trained model	Uploading an *.h5 file, i.e. a neural network model, to the Google Colab server, which eliminates the need to retrain the network and reduces the operating time
Testing the network on another set	Testing the network after training. Images of files outside the training set are fed to the input, the neural network processes the images and generates an output file in the form of an image with restored clusters
Intersection over Union (IoU)	Testing the original and neural network-generated images using the IoU method [109]

The software code for working with the training set of photographic images of fragments of obtained nuclear emulsion was divided into several modules, each executing its particular task (Table 2).

To solve the formulated problem with the chosen neural network architecture, eight epochs of training were required. The pure network training time amounted to ~ 1.5 h. After each epoch, the accuracy of the model operation changed, and towards the end of the work a worsening tendency appeared. After the end of neural network operation, the program chose the variant with the best accuracy. The accuracy obtained in different epochs is presented in Fig. 37.

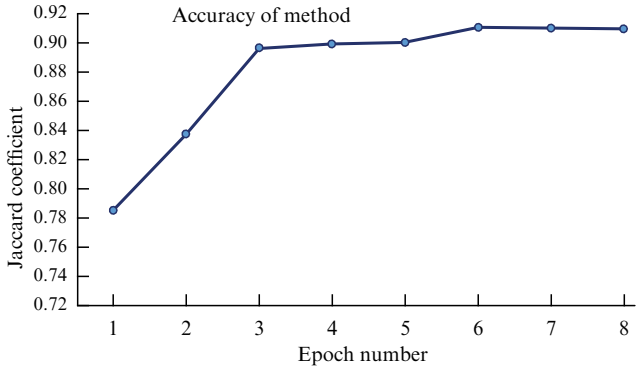

Figure 37. Accuracy of model for different training epochs.

The best value of the Jaccard coefficient (~ 0.912) was obtained in epoch 6. In epochs 7 and 8, an overtraining of the network occurred. Therefore, with the existing training set of images, it is impossible to reach higher accuracy.

After the neural network training, its operation was checked using additional images not included in the training set. For each testing, the intersection over union (IoU) method of comparing images was used. Figure 38 demonstrates the work of the neural network on reconstructing the clusters obtained after its training when the initial image is not taken from the training set. The coincidence with the initial image reaches $\sim 93\%$. Increasing the number of images in the training set will lead to increasing the accuracy of the neural network operation on reconstructing the cluster images; however, it will require large random access memory resources and disk space.

The results of this work were presented at the XVI Cherenkov Session, New Methods in Experimental Nuclear and Particle Physics [110].

In the future, it is planned to implement a block for image processing and cluster selection using a neural network in the working PAVICOM software package. For this purpose, it will be necessary to create the executed module for image segmentation written in the Python language and to embed it into the program complex written in C^{++}. Upon successful implementation of this software code and subsequent testing on a new generation of scanning stations, further upgrade of the software code and training of the convolutional neural network with the 3D U-Net architecture using a set of images reproducing a three-dimensional object is planned.

Thus, the LEP team continuously modernizes the PAVIKOM measuring complex, expanding its technical and analytical capabilities, as a result of which the range of experiments carried out and the speed and quality of processing the obtained data increases.

5. Conclusion. Prospects of track technique development at Laboratory of Elementary Particles

The progress in nuclear physical track technique opens possibilities of unique investigations in the field of modern fundamental physics, as well as allowing the development of new approaches to solving a wide range of applied problems of primary importance.

Track detectors possessing the highest spatial resolution and, therefore, capable of separating particle tracks played a noticeable role in the development of experimental nuclear physics due to the clarity of data presentation and the possibility of obtaining a thorough spatial pattern of the processes studied. The track technique is applied in the physics of high energies and cosmic rays, astrophysics, and applied research by the muonography method.

Of primary importance are the technologies providing fast and high-quality processing of data from track detectors, in particular, automated scanning microscopes, which have been actively developed in the last 25 years. Earlier, the processing of data from these integrated track detectors, performed manually with optical microscopes, required huge amounts of labor and time, and the lack of a high speed of such processing allowed no sufficient statistical provision of data. The method of automated measurements practiced at present has led to an increase in the processing speed by more than three orders of magnitude and, consequently, allowed processing large arrays of experimental data, substantially enhancing the statistics of events. The introduction of optical automated complexes, operating with software packages based on object-oriented programming, allows moving to a higher level of performing experiments using the track technique of particle registration and substantially extends the range of problems where it can be used. It should be noted that there are no universal algorithms for image processing in track detectors, which requires the continual creation of new original algorithms, including those based on artificial neural networks, allowing for specific features of the experiment and the characteristics of particle tracks.

Of great interest is the use of track detectors based on photographic nuclear emulsion for a number of applied tasks, in particular, for noninvasive study of the internal structure of large natural and industrial sites, as well as in performing exploration work by muonography. The method consists of

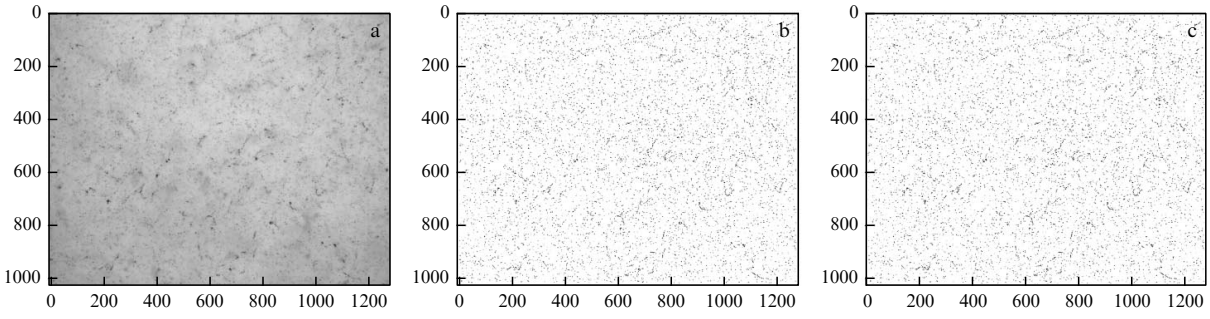

Figure 38. Image beyond training set: (a) original image of 1280×1024 pixels obtained at PAVICOM-3 measuring complex; (b) clusters reconstructed using a graphics processor, (c) clusters reconstructed using a neural network.

recording the degree of absorption of cosmic muon fluxes passing through the substance of the object being studied [111]. The relevance of the method is evidenced by a wide range of problems that can be solved by applying it: monitoring large natural phenomena (volcanos, geological plates, karst caves, etc.), nondestructive control of industrial sites (mines and excavations, nuclear power plants, industrial and building sectors), monitoring of flamable carbon dumps, analysis of seismic processes. The method can also be used as a promising addition to traditional geophysical methods of mineral exploration. Of separate interest are the studies of archeological artifacts without the risk of damaging them. The fact that the muonography method allows solving these problems in an available and safe way has been demonstrated in many studies carried out by LEP researchers in recent years [105, 106, 112], in which results of primary importance have been obtained. A combination of renewed production of nuclear emulsion in Russia and the presence of high-technology scanning instrumentation created conditions for the development and wide application of the muonography technique — an efficient and economical, ecologically safe method of research in many fields of scientific and practical activity.

Thus, the experience and qualifications of LEP researchers have found application in a number of very important experiments; the results of some of them are described in the present review. The methods and approaches used by researchers from the Laboratory of Elementary Particles, the traditional combination of experimental activity and theoretical developments, and the outstanding educational activities — the fusion of these factors is the basis for studies of the track technique successfully developed over a few decades and planned for the future.

The study was supported by the Russian Science Foundation within the program Conducting Fundamental Scientific Research and Exploratory Scientific Research by Individual Scientific Teams (Project No. 23-12-00054).

References

1. Daion M I, Merzon G I, Fedorov V M (Comp.) *Artem Alikhanyan. Ocherki, Vospominaniya, Dokumenty* (Artem Alikhanyan. Essays, Memoirs, Documents) (Moscow: RIIS FIAN, 2000)
2. Mamidzhanyan E A, Merzon G I (Eds–Comp.) *Artem Alikhanyan v Vospominaniyakh Druzei i Kolleg* (Artem Alikhanyan in the Memories of Friends and Colleagues) (Moscow: Fizmatlit, 2008)
3. Landau L *J. Phys. USSR* **8** 201 (1944); Landau L D, in *Sobranie Trudov* (Collected Works) Vol. 1 (Ed. E M Lifshitz) (Moscow: Nauka, 1969) p. 482
4. Alikhanyan A I, in *Problemy Yadernoi Fiziki i Fiziki Elementarnykh Chastits*: *Sbornik Statei, Posvyashchennykh Pamyati Akademika A I Alikhanova* (Problems of Nuclear Physics and Elementary Particle Physics: Collection of Articles Dedicated to the Memory of Academician A I Alikhanov) (Ed. L B Okun) (Moscow: Nauka, 1975) p. 3
5. Ariga A et al., in *Particle Physics Reference Library* Vol. 2 (Eds C W Fabjan, H Schopper) (Cham: Springer, 2020) p. 383, https://doi.org/10.1007/978-3-030-35318-6_9
6. The SHiP Collab., Ahdida C et al. *JINST* **17** P03013 (2022) https://doi.org/10.1088/1748-0221/17/03/P03013
7. Chernyavskiy M M et al. *JINST* **17** P02002 (2022) https://doi.org/10.1088/1748-0221/17/02/P02002
8. Agafonova N et al. (OPERA Collab.) *Phys. Rev. Lett.* **120** 211801 (2018)
9. Kaplon M, Peters B, Ritson D M *Phys. Rev.* **85** 900 (1952)
10. Niu K, Mikumo E, Maeda Y *Prog. Theor. Phys.* **46** 1644 (1971) https://doi.org/10.1143/PTP.46.1644
11. DONUT Collab., Kodama K et al. *Phys. Lett. B* **504** 218 (2001)
12. Agafonova N et al. *JINST* **4** P06020 (2009) https://doi.org/10.1088/1748-0221/4/06/P06020
13. The ATLAS Collab., Aad G et al. *JINST* **3** S08003 (2008) https://doi.org/10.1088/1748-0221/3/08/S08003
14. Boldyrev A S et al. *Instrum. Exp. Tech.* **55** 323 (2012); *Prib. Tekh. Eksp.* (3) 27 (2012)
15. Ginzburg V L, Frank I M *J. Phys. USSR* **9** 353 (1945); *Zh. Eksp. Teor. Fiz.* **16** 15 (1946)
16. Dolgoshein B *Nucl. Instrum. Meth. Phys. Res. A* **326** 434 (1993) https://doi.org/10.1016/0168-9002(93)90846-A
17. he ATLAS TRT Collab., Abat A et al. *JINST* **3** P06007 (2008) https://doi.org/10.1088/1748-0221/3/06/P06007
18. Cornelissen T et al. *J. Phys. Conf. Ser.* **119** 032014 (2008)
19. ATLAS Collab., Aad G et al. *Phys. Lett. B* **716** 1 (2012)
20. Boos E G et al., Experiments at CERN in 1996 (Geneva: CERN, 1996) p. 122
21. Dobrotin N A et al. *Bull. Russ. Acad. Sci. Phys.* **63** 393 (1999); *Izv. Ross. Akad. Nauk. Ser. Fiz.* **63** 485 (1999)
22. Dremin I M, Kaidalov A B *Phys. Usp.* **49** 263 (2006); *Usp. Fiz. Nauk* **176** 275 (2006)
23. Kotel'nikov K A et al. *Nauka — Proizvodstvu* (12) 29 (2000)
24. Dremin I M et al. *Phys. Lett. B* **499** 97 (2001)
25. Dremin I M, Ivanov O V, Nechitailo V A *Phys. Usp.* **44** 447 (2001); *Usp. Fiz. Nauk* **171** 465 (2001)
26. Polukhina N G ''Issledovaniya aktual'nykh problem yadernoi fiziki na osnove metodiki polnost'yu avtomatizirovannoi obrabotki trekovykh detektorov na mnogofunktsional'noi ustanovke PAVIKOM'' (''Study of current problems of nuclear physics based on the methodology of fully automated processing of track detectors on the multifunctional PAVIKOM facility''), Thesis ... of Doctor of Physical and Mathematical Sciences (Moscow: LPI, 2006)
27. Apanasenko A V et al. *JETP Lett.* **30** 145 (1979); *Pis'ma Zh. Eksp. Teor. Fiz.* **30** 157 (1979)
28. Agafonova N et al. *Eur. Phys. J. C* **74** 2986 (2014)
29. Agafonova N et al. *Phys. Lett. B* **691** 138 (2010)
30. Agafonova N et al. (OPERA Collab.) *Phys. Rev. Lett.* **115** 121802 (2015)
31. Polukhina N, Konovalova N, Shchedrina T *Physics* **5** 499 (2023)
32. Acampora G et al. *JINST* **19** P05067 (2024); arXiv:2210.02784
33. Di Crescenzo A ''Neutrino expectations at advanced SND@LHC,'' Report on 14th SND@LHC Collaboration Meeting, 4–7 Sept. 2023
34. Roesler S, Engel R, Ranft J, in *Advanced Monte Carlo for Radiation Physics, Particle Transport Simulation and Applications* (Eds A Kling et al.) (Berlin: Springer, 2001) p. 1033, https://doi.org/10.1007/978-3-642-18211-2_166
35. Ahdida C et al. *Front. Phys.* **9** 788253 (2022) https://doi.org/10.3389/fphy.2021.788253
36. Albanese R et al. (SND@LHC Collab.) *Phys. Rev. Lett.* **131** 031802 (2023)
37. Kaplon M F et al. *Phys. Rev.* **88** 295 (1952)
38. The JACEE Collab., Burnett T H et al. *Nucl. Instrum. Meth. Phys. Res. A* **251** 583 (1986)
39. RUNJOB Collab., Apanasenko A V et al. *Astropart. Phys.* **16** 13 (2001)
40. Osedlo V I et al., in *Proc. 30th Intern. Cosmic Ray Conf., ICRC 2007* Vol. 4 (Mexico: Yucatan Autonoma Univ., 2007) p. 667
41. Osedlo V I et al., in *Proc. 30th Intern. Cosmic Ray Conf., ICRC 2007* Vol. 4 (Mexico: Yucatan Autonoma Univ., 2007) p. 663
42. Managadze A K et al. *Bull. Russ. Acad. Sci. Phys.* **71** 513 (2007); *Izv. Ross. Akad. Nauk Ser. Fiz.* **71** 530 (2007)
43. Managadze A K ''Osobennosti prostranstvennykh kharakteristik yadernykh vzaimodeistvii kosmicheskikh luchei sverkhvysokikh energii'' (''Features of spatial characteristics of nuclear interactions of ultra-high energy cosmic rays''), Thesis ... of Doctor of Physical and Mathematical Sciences (Moscow: MSU SINP, 2010)
44. Lokhtin I P, Managadze A K, Snigirev A M *Phys. Atom. Nucl.* **76** 602 (2013) https://doi.org/10.1134/S1063778813040078; *Yad. Fiz.* **76** 645 (2013) https://doi.org/10.7868/s0044002713040089
45. Pavlyuchenko V P *Izv. Ross. Akad. Nauk Ser. Fiz.* **63** 457 (1999)
46. Ginzburg V L et al. *Dokl. Phys.* **50** 283 (2005); *Dokl. Ross. Akad. Nauk* **402** 1 (2005)

47. Cecchini S et al., in *Proc. 16th ESA Symp. on European Rocket and Balloon Programmes and Related Research* (Ed. B Warmbein) (Noordwijk: ESA Publ. Division, 2003) p. 529
48. Fowler P H et al. *Astrophys. J.* **314** 739 (1987)
49. Binns W R et al. *Astrophys. J.* **346** 997 (1989)
50. Weaver B A, Westphal A J *Astrophys. J.* **569** 493 (2002)
51. Donnelly J et al. *Astrophys. J.* **747** 40 (2012)
52. Bagulya A V et al. *Bull. Lebedev Phys. Inst.* **42** 152 (2015) https://doi.org/10.3103/S1068335615050073; *Kratk. Soobshch. Fiz.* **42** (5) 49 (2015)
53. Aleksandrov A B et al. *Bull. Lebedev Phys. Inst.* **40** 126 (2013) https://doi.org/10.3103/S1068335613050059; *Kratk. Soobshch. Fiz.* **40** (5) 29 (2013)
54. Horn P, Maurette M, Von Oertzen W *Z. Naturforsch. A* **22** 1793 (1967) https://doi.org/10.1515/zna-1967-1117
55. Flerov G N, Ter-Akopian G M *Pure Appl. Chem.* **53** 909 (1981) https://doi.org/10.1351/pac198153050909
56. Aleksandrov A B et al. *Vestn. Otd. Nauk Zemle Ross. Akad. Nauk* **1** NZ2003 (2009); 10.2205/2009NZ000003
57. Alexeev V et al. *Astrophys. J.* **829** 120 (2016)
58. Bagulya A V et al. *JETP Lett.* **97** 708 (2013) https://doi.org/10.1134/S0021364013120047; *Pis'ma Zh. Eksp. Teor. Fiz.* **97** 811 (2013)
59. Tan Naing So "Obluchennye kosmicheskimi luchami meteoritnye oliviny kak instrument poiska sverkhtyazhelykh elementov v prirode" ("Cosmic ray irradiated meteorite olivines as a tool for searching for superheavy elements in nature"), Thesis ... of Doctor of Physical and Mathematical Sciences (Moscow: FIAN, 2022)
60. Alexandrov A et al. *Adv. Space Res.* **70** 2674 (2022)
61. Alexandrov A B et al. *Phys. At. Nucl.* **85** 446 (2022) https://doi.org/10.1134/S1063778822050039
62. Komarov F F *Phys. Usp.* **60** 435 (2017); *Usp. Fiz. Nauk* **187** 465 (2017); 10.3367/UFNr2016.10.038012
63. Medvedev N et al. *J. Appl. Phys.* **133** 100701 (2023)
64. Price P B et al. *Phys. Rev.* **164** 1618 (1967)
65. Perron C et al. *Int. J. Radiat. Appl. Instrum. D Nucl. Tracks Radiat. Meas.* **15** 231 (1988) https://doi.org/10.1016/1359-0189(88)90137-9
66. Green P F, Bull R K, Durrani S A *Nucl. Instrum. Meth.* **157** 185 (1978)
67. Villa F et al. *Radiat. Meas.* **28** 543 (1997)
68. Dalton H et al. *Chem. Geol.* **558** 119899 (2020)
69. Spohr R et al. *Nucl. Instrum. Meth. Phys. Res. B* **268** 676 (2010)
70. Kozhina E P et al. *Appl. Sci.* **11** 1375 (2021)
71. Choudhury N, Singh F, Sarma B K *Radiat. Eff. Defects Solids* **168** 498 (2013)
72. Kamaev G N et al. *Proc. SPIE* **11022** 1102213 (2019) https://doi.org/10.1117/12.2522161
73. Pompos A, Durante M, Choy H *JAMA Oncol.* **2** 1539 (2016) https://doi.org/10.1001/jamaoncol.2016.2646
74. Gunderson L L, Tepper J E *Clinical Radiation Oncology* (Cham: Elsevier, 2015) e-book
75. Cucinotta F A, To K, Cacao E *Life Sci. Space Res.* **13** 1 (2017) https://doi.org/10.1016/j.lssr.2017.01.005
76. Douki T et al. *Int. J. Radiat. Biol.* **82** 119 (2006)
77. Ferruz M B et al., in *Nanoscale Insights into Ion-Beam Cancer Therapy* (Ed. A Solov'yov) (Cham: Springer, 2017) p. 379, https://doi.org/10.1007/978-3-319-43030-0_12
78. Murat M, Akkerman A, Barak J *IEEE Trans. Nucl. Sci.* **55** 3046 (2009) https://doi.org/10.1109/TNS.2008.2007646
79. Tracy C L et al. *Nat. Commun.* **6** 6133 (2015)
80. Ziegler J F, Biersack J P, Littmark U *The Stopping and Range of Ions in Solids* (New York: Pergamon Press, 1985)
81. Medvedev N A, Rymzhanov R A, Volkov A E *J. Phys. D* **48** 355303 (2015)
82. Medvedev N, Volkov A E *J. Phys. D* **53** 235302 (2020)
83. Szenes G *Nucl. Instrum. Meth. Phys. Res. B* **298** 76 (2013)
84. Itoh N, Marshall Stoneham A *Nucl. Instrum. Meth. Phys. Res. B* **146** 362 (1998)
85. Yavlinskii Yu N *Nucl. Instrum. Meth. Phys. Res. B* **166–167** 35 (2000)
86. Miterev A M *Phys. Usp.* **45** 1019 (2002); *Usp. Fiz. Nauk* **172** 1131 (2002)
87. Kaganov M I, Lifshitz I M, Tanatarov L V *Sov. Phys. JETP* **4** 173 (1957); *Zh. Eksp. Teor. Fiz.* **31** 232 (1956)
88. Toulemonde M, Dufour C, Paumier E *Phys. Rev. B* **46** 14362 (1992)
89. Medvedev N et al. *Adv. Theory Simul.* **5** 2200091 (2022) https://doi.org/10.1002/adts.202200091
90. Rymzhanov R A, Medvedev N A, Volkov A E *Nucl. Instrum. Meth. Phys. Res. B* **388** 41 (2016)
91. Medvedev N A, Rymzhanov R A, Volkov A E *J. Phys. D* **48** 355303 (2015)
92. Medvedev N, Volkov A E *J. Appl. Phys.* **131** 225903 (2022)
93. Rymzhanov R A et al. *Nucl. Instrum. Meth. Phys. Res. B* **440** 25 (2019)
94. Tsujii H *J. Phys. Conf. Ser.* **777** 012032 (2017)
95. Gorbunov S A et al. *Nucl. Instrum. Meth. Phys. Res. B* **365** 656 (2015)
96. Gorbunov S A et al. *J. Phys. D* **50** 395306 (2017)
97. Gorbunov S A, Rymzhanov R A, Volkov A E *Sci. Rep.* **9** 15325 (2019)
98. Gorbunov S A et al. *J. Phys. Chem. C* **127** 5090 (2023)
99. Aleksandrov A B et al. *Nucl. Instrum. Meth. Phys. Res. A* **535** 542 (2004)
100. Aleksandrov A B et al. *Russ. Phys. J.* **50** 1026 (2007) https://doi.org/10.1007/s11182-007-0148-7; *Izv. Vyssh. Uchebn. Zaved. Fiz.* (10) 61 (2007)
101. Alexandrov A et al. *Measurement* **187** 110244 (2022)
102. Alexandrov A, De Lellis G, Tioukov V *Sci. Rep.* **9** 2870 (2019)
103. Alexandrov A, Vladymyrov M, Tioukov V *Zenodo* (2020) https://doi.org/10.5281/zenodo.4385773
104. Tioukov V et al. *Nucl. Instrum. Meth. Phys. Res. A* **559** 103 (2006)
105. Alexandrov A B et al. *Phys. Part. Nucl.* **53** 1146 (2022) https://doi.org/10.1134/S1063779622060028; *Fiz. Elem. Chast. At. Yad.* **53** 1423 (2022)
106. Alexandrov A et al., Preprints 2023090820 (2023) https://doi.org/10.20944/preprints202309.0820.v1
107. Ronneberger O, Fischer P, Brox T, in *Medical Image Computing and Computer–Assisted Intervention — MICCAI 2015* (Lecture Notes in Computer Science, Vol. 9351, Eds N Navab et al.) (Cham: Springer, 2015) p. 234, https://doi.org/10.1007/978-3-319-24574-4_28; arXiv:1505.04597
108. Lin T-Y et al., arXiv:1708.02002, Subjects: Computer Vision and Pattern Recognition (2018)
109. Intersection over Union (IoU). CloudFactory Ltd, https://hasty.ai/docs/mp-wiki/metrics/iou-intersection-over-union
110. Vasil'ev V T et al. "Neironnye seti dlya obrabotki yadernykh emul'sii" ("Neural networks for processing nuclear emulsion"), in *XVI Cherenkovskie Chteniya: Novye Metody v Eksperimental'noi Yadernoi Fizike i Fizike Chastits, Moskva, FIAN, 18 Aprelya 2023 g.* (XVI Cherenkov Readings: New Methods in Experimental Nuclear Physics and Particle Physics, Moscow, LPI, April 18, 2023), https://x4u.lebedev.ru/che2023/program_ru-RU.html; *Yad. Fiz. Inzhiniring* **15** (1) 31 (2024) https://doi.org/10.56304/S2079562923010293
111. Aleksandrov A B et al. *Phys. Usp.* **60** 1277 (2017); *Usp. Fiz. Nauk* **187** 1375 (2017)
112. Aleksandrov A B et al. *J. Exp. Theor. Phys.* **134** 506 (2022) https://doi.org/10.1134/S106377612204001X; *Zh. Eksp. Teor. Fiz.* **161** 590 (2022)